FEDERAL UNIVERSITY OF PARAIBA

DEPARTMENT OF PHYSICS

DOCTORAL THESIS

Yohan Mauricio Oviedo Torres

Search for new physics at the LHC and Future Colliders

João Pessoa, Paraíba, Brazil

August 15, 2023

Yohan Mauricio Oviedo Torres

Search for new physics at the LHC and Future Colliders

Thesis presented to the Graduate Program in
Physics of the Federal University of Paraiba,
as part of the requirements to obtain the
Degree of Doctor of Physics. Research Field:
Particle Physics.

Supervisor: Dr. Farinaldo da Silva Queiroz

Co-supervisor: Dr. Alexandre Alves

João Pessoa, Paraíba, Brazil

August 15, 2023

Universidade Federal da Paraíba
Centro de Ciências Exatas e da Natureza
Programa de Pós-Graduação *Stricto Sensu* em Física

Ata da Sessão Pública da Defesa de tese de Doutorado do aluno Yohan Maurício Oviedo Torres, candidato ao Título de Doutor em Física na Área de Concentração Física de Partículas Elementares e Campos.

Aos vinte e sete dias do mês de outubro do ano de dois mil e vinte e três, às 14h00, na sala virtual https://meet.google.com/vcp-oaxj-uuf, reuniram-se os membros da Banca Examinadora constituída para avaliar a tese de Doutorado, na área de Física de Partículas Elementares e Campos, de **Yohan Maurício Oviedo Torres**. A banca foi composta pelos(as) professores(as) doutores(as): Farinaldo da Silva Queiroz (PPGF/UFPB), orientador e presidente da banca examinadora, Dionísio Bazeia Filho (PPGF/UFPB), Paulo Sérgio Rodrigues da Silva (PPGF/UFPB), Luciano Melo Abreu (UFBA) e José Abdalla Helayël-Neto (CBPF). Dando início aos trabalhos, o Prof. Farinaldo da Silva Queiroz comunicou aos presentes a finalidade da reunião. A seguir, passou a palavra para o candidato para que o mesmo fizesse, oralmente, a exposição da pesquisa de tese intitulada "*Busca Por Física Nova no LHC e Futuros Colisores*". Concluída a exposição, o candidato foi arguido pela Banca Examinadora, que emitiu o parecer **"aprovado".** Assim sendo, deve a Universidade Federal da Paraíba expedir o respectivo diploma de Doutor em Física na forma da lei. E para constar, Danilo Wilson Lemos Menezes, Técnico em Assuntos Educacionais, redigiu a presente ata que vai assinada pelos membros da Banca Examinadora. João Pessoa, Paraíba, **27 de outubro de 2023**.

Prof. Dr. Farinaldo da Silva Queiroz
Orientador - PPGF/UFPB

Prof. Dr. Dionísio Bazeia Filho
PPGF/UFPB

Prof. Dr. Paulo Sérgio Rodrigues da Silva
PPGF/UFPB

Prof. Dr. José Abdalla Helayël-Neto
CBPF

Prof. Dr. Luciano Melo Abreu
UFBA

Dedico esta tese à minha família, amigos e meu grande amor, pela fé, confiança e paciência demonstrada. Também dedico esta tese a todas as pessoas que colocaram uma parte do seu coração numa mala e deixaram o seu país para realizar os seus sonhos.

Acknowledgements

As coisas têm vida própria, tudo é questão de despertar a sua alma.

(Gabriel García Marquez, Cem anos de solidão)

List of Publications

- D. Cogollo, **Yohan M. Oviedo-Torres**, Yoxara S. Villamizar. Are 3-4-1 models able to explain the upcoming results of the muon anomalous magnetic moment?, Int.J.Mod.Phys.A, v. 35, n. 23, 2050126, 2020. DOI: 10.1142/S0217751X20501262

- D. Cogollo, F.F. Freitas, C.A. de S. Pires, **Yohan M. Oviedo-Torres**, P. Vasconcelos. Deep learning analysis of the inverse seesaw in a 3-3-1 model at the LHC, Phys. Lett. B., v. 811, 135931, 2022. DOI: 10.1103/PhysRevD.106.055027

- A. Alves, L. Duarte, S. Kovalenko, **Y.M. Oviedo-Torres**, F.S. Queiroz, Y.S. Villamizar. Constraining 3-3-1 models at the LHC and future hadron colliders, Phys. Rev. D., v. 106, n. 5, 055027, 2022. DOI: 10.1103/PhysRevD.106.055027

- A.E. Cárcamo Hernández, L. Duarte, A.S. de Jesus, S. Kovalenko, F.S. Queiroz, C. Siqueira, **Y.M. Oviedo-Torres**, Y. Villamizar. Flavor changing interactions confronted with meson mixing and hadron colliders, Phys. Rev. D, v. 107, n. 6, 063005, 2023. DOI: 10.1103/PhysRevD.107.063005

List of pre-prints

- S. Kovalenko, A.S. de Jesus, A.R. Zerwekh, **Y.M. Oviedo-Torres**, F.S. Queiroz, T.B. de Melo, J.P. Neto, Y.S. Villamizar. On the Role of LHC and HL-LHC in Constraining Flavor Changing Neutral Currents, e-Print: 2304.00041 [hep-ph], 2023.

- Giorgio Arcadi, Glauber C. Dorsch, Jacinto P. Neto, Farinaldo S. Queiroz, **Y.M. Oviedo-Torres**. Probing a Dark Sector with Collider Physics, Direct Detection, and Gravitational Waves, e-Print: 2307.06376 [hep-ph], 2023.

- A. Alves, G. Gil da Silveira, V. P. Gonçalves, F.S. Queiroz, **Y.M. Oviedo-Torres**, J. Zamora-Saa. Searching for a Leptophilic Z' and a 3-3-1 symmetry at CLIC, e-Print: 2309.00681 [hep-ph], 2023.

- D. Cogollo, M.J. Neves, Tessio B. de Melo, Alvaro S. de Jesus, **Y.M. Oviedo-Torres**, F.S. Queiroz. Constraints on Hidden Sectors Using Rare Kaon Decays, e-Print: 2310.19959 [hep-ph], 2023.

Abstract

É quase um consenso geral que o modelo padrão da física de partículas não é a teoria final que descreve as interações fundamentais entre partículas elementares. Isso ocorre porque diferentes observações experimentais sugerem de forma convincente que a teoria padrão precisa ser estendida. Problemas como a necessidade de um candidato à matéria escura, a massa do neutrino, hierarquia, assimetria matéria-antimatéria, entre outros, apontam em uma direção muito clara: buscas experimentais por sinais de física além do modelo padrão em experimentos de baixas e altas energias são urgentemente necessários. Dentro dos tipos de experimentos de alta energias, os colisores de partículas certamente desempenham um papel fundamental nessa tarefa pois são máquinas que podem acelerar partículas a velocidades próximas à velocidade da luz e, consequentemente, são capazes de gerar colisões de altíssima energia, suficientes para, por exemplo, produzir novas partículas que não estão dentro do espectro de partículas do modelo padrão.

Motivados por esses problemas em aberto e pelo enorme potencial dos colisores de partículas para testar teorias além do modelo padrão, nesta tese abordaremos o estudo de um novo bóson Z' sob duas perspectivas diferentes. Na primeira parte desta tese faremos um estudo detalhado do modelo padrão que servirá de base para apresentar as extensões do modelo padrão que iremos utilizar. Na segunda parte, usaremos dados da colaboração ATLAS para restringir a massa de um novo bóson Z' na configuração atual do Large Hadron Collider (LHC) para os modelos 3-3-1 com neutrinos de mão direita (331RHN) e 3-3-1 com léptons neutros pesados (331LHN). Uma vez encontrados esses limites, vamos extrapolá-los para as esperadas atualizações de alta luminosidade e alta energia do LHC conhecidas como HL-LHC e HE-LHC, respectivamente, bem como o experimento Future Circular Collider (FCC) projetado para funcionar após o LHC. Para a terceira parte desta tese, realizaremos um estudo de sensibilidade no experimento Compact Linear Collider (CLIC), no qual obteremos a luminosidade que necessita o experimento para detectar um novo bóson Z' dos modelos 331RHN, 331LHN e o Z' leptofílico. Para fazer isso, compararemos um grande número de eventos de sinal e de fundo para encontrar os melhores cortes cinemáticos nos quais poderemos ver um sinal de um Z' com 95% C.L. ou a descoberta de um Z' com 5σ de significância estatística.

Palavras-chave: Colisor de Partículas; 331RHN; 331LHN; Leptofilico; LHC; ATLAS; FCC; Futuros Colisores; CLIC.

Abstract

It is almost a general consensus that the standard model of particle physics is not the final theory that describes the fundamental interactions between elementary particles. This is because different experimental observations convincingly suggest that the standard theory needs to be extended. Problems such as the need for a candidate for dark matter, the neutrino mass, hierarchy, matter-antimatter asymmetry, among others, point in a very clear direction: experimental searches for signs of physics beyond the standard model in experiments of low and high energies are necessarily urgent. Within the types of high-energy experiments, particle colliders certainly play a fundamental role in this task, since they are machines that can accelerate particles to speeds close to the speed of light and, consequently, are capable of generating very high-energy collisions, enough energy to, for example, produce new particles that are not in the particle spectrum of standard model.

Motivated by these open problems and by the enormous potential of particle colliders to test theories beyond the standard model, in this thesis we will approach the study of a new Z' boson from two different perspectives. In the first part of this thesis we will have a detailed study of the standard model that will serve as a basis for presenting the extensions of the standard model that we are going to use. In the second part, we will use data from the ATLAS collaboration to constrain the mass of a new Z' boson using the current LHC configuration for 3-3-1 with right-handed neutrinos and 3-3-1 with heavy neutral leptons models. Once these limits are found, we are going to extrapolate them to the expected updates of high luminosity and high energy of the LHC known as HL-LHC and HE-LHC, respectively, as well as the Future Circular Collider (FCC) projected to work after the LHC. For the third part of this thesis, we will carry out a sensitivity study in the Compact Linear Collider (CLIC) experiment, in which we will obtain the luminosity that the experiment needs to detect a new Z' boson of the 331RHN, 331LHN and Z' leptophilic models. To do this, we will compare a large number of signal and background events to find the best kinematic cuts in which we can see a Z' signal with 95% C.L. or the discovery of a Z' with 5σ statistical significance.

Keywords: Particle Collider; 331RHN; 331LHN; Leptophilic; LHC; ATLAS; FCC; Future Colliders; CLIC.

List of Figures

List of Tables

List of abbreviations and acronyms

331LHN	3-3-1 model with heavy neutral lepton
331RHN	3-3-1 model with right-handed neutrinos
ATLAS	A Toroidal LHC Apparatus
BM	Benchmark
BSM	Beyond the Standard Model
CDR	Conceptual Design Report
CERN	European Organization for Nuclear Research
CKM	Cabibbo-Kobayashi-Maskawa
CLIC	Compact Linear Collider
CMS	Compact Muon Solenoid
C.L.	Conficende Level
DM	Dark Matter
DY	Drell-Yan
FCC	Future Circular Collider
FCC-hh	Future Circular Collider using Hadron-Hadron beams
LEP	Large Electron-Positron Collider
LHC	Large Hadron Collider
NP	New Physics
NRQM	Non-Relativistic Quantum Mechanics
PDF	Parton Distribution Function
QED	Quantum Electrodynamics
QFT	Quantum Field Theory
RQM	Relativistic Quantum Mechanics

SM   Standard Model

SLAC   Stanford Linear Accelerator Center

SSB   Spontaneous Symmetry Breaking

VEV   Vacuum Expectation Value

Contents

1 Introduction

Over the past century, the standard model of particle physics (SM) has emerged as a remarkably successful theoretical framework that describes elementary particles and their fundamental interactions. However, as our understanding of the universe deepens and experimental precision improves, certain gaps and limitations within the SM have become increasingly apparent. These gaps, such as the lack of a viable dark matter (DM) candidate, the inability to incorporate gravity, and the absence of an explanation for neutrino masses, among others, have spurred the scientific community to explore new avenues of knowledge.

The path towards addressing these challenges has led to consider theories that extend beyond the boundaries of the SM. These theories, often collectively referred to as "Beyond the Standard Model" (BSM) theories, propose new particles, interactions and symmetries that could potentially bridge the existing gaps and provide a more comprehensive understanding of the fundamental forces that govern the universe. These new theoretical frameworks tend to be simple or complex extensions of the SM symmetry group and hold the promise of addressing some of the most pressing questions in particle physics.

Central to the exploration of BSM particle physics is the utilization of high-energy particle colliders. Particle colliders play a crucial role in advancing our understanding of the subatomic world by enabling scientists to recreate extreme conditions that existed in the early universe, moments after the Big Bang. These state-of-the-art machines, such as the Large Hadron Collider (LHC) at CERN, have the capability to accelerate particles to velocities close to the speed of light and collide them with unprecedented energy. Through these collisions, we can probe the fundamental building blocks of matter at scales never before possible, potentially revealing the existence of new particles or interactions predicted by BSM theories. So far, particle colliders like the LHC have not shown signs of new physics (NP) and this has served as motivation for planning upgrades to the LHC or creating future colliders like the High-Luminosity LHC (HL-LHC), High-Energy LHC (HE-LHC), Future Circular Collider (FCC) and the Compact Linear Collider (CLIC).

Due to the need for physics models BSM and the fundamental role that particle colliders have for the exploration of this new physics, in this thesis we will deepen the study of a new Z' vector boson that arises from three very popular models in the literature. The first two are simple extensions of the SM symmetry group and are po-

pularly known as 3-3-1 models. Specifically we will study the models known as the 3-3-1 with heavy neutral leptons (331LHN) and the 3-3-1 with right-handed neutrinos (331RHN). On the other hand, the other model that we will study will be the Z' leptophilic.

The first part that corresponds to the second chapter of this thesis will be a detailed review of the standard model of particle physics. The second part corresponding to the third chapter will focus on using data from the current LHC to put lower mass bounds on the mass of a new Z' and extrapolate these bounds for future colliders such as the HL-LHC, HE-LHC and the FCC. The third part corresponding to the fourth chapter will be a sensitivity study to detect a new Z' in the CLIC, in which we will study the capacity that the experiment could have to detect this new boson within the two models 3-3-1 explored in the second part, as well as a leptophilic Z'. In the last part we will present the conclusions.

2 The Standard Model of Particle Physics

The beginning of the 20th century witnessed profound and revolutionary changes in physics, marked by the development of two great physical theories: general relativity, describing physics on large scales, and non-relativistic quantum mechanics (NRQM), explaining phenomena on small scales. NRQM played a crucial role in providing mathematical frameworks to describe new phenomena related to atoms and molecules, which clearly deviated from classical physics laws. However, NRQM was not enough to explain certain physical phenomena, such as relativistic bound states, inelastic (transmutation) scattering, decay of composite and elementary particles, and vacuum energy [1].

Currently, all these relativistic quantum phenomena are well explained by relativistic quantum mechanics (RQM) or, in a more general framework, quantum field theory (QFT)[1]. In that sense, QFT has proven to be a powerful tool for describing the interactions among the fundamental constituents of matter [2]. In conjunction with group theory, it has enabled the construction of the framework known today as the Standard Model of Particle Physics (SM).

The SM is considered one of the most significant milestones in physics during the twentieth century, as it successfully describes three of the four fundamental interactions in nature: the strong, electromagnetic, and weak interactions[2][3]. This theoretical framework is a gauge theory based on the local gauge symmetry group $SU(3)_C \times SU(2)_L \times U(1)_Y$, where the subscripts C, L, and Y denote Color, left-handed chirality, and weak hypercharge, respectively.

Before delving into the SM lagrangian, we will provide a brief overview of the concept of gauge invariance in quantum electrodynamics (QED) and the $SU(2)$ Yang-Mills theory. These two theories will serve as the fundamental building blocks of the SM.

---

[1] The distinction between NRQM, RQM, and QFT lies in their respective natures. NRQM is a non-relativistic quantum particle theory, RQM is also a quantum particle theory but incorporates the principles of special relativity, while QFT is a quantum relativistic theory of fields.

[2] Since the strong interaction remains unbroken and there is no mixing between the electroweak sector, this thesis will solely focus on the unified theory of the weak and electromagnetic interactions known as electroweak interactions

2.1   The Gauge Invariance in Quantum Field Theories

We say that the SM is a local gauge theory because it is based on the Gauge Principle [4]. This principle involves a transformation that can be applied to the fields and potentials used to describe a physical system[3] without altering the predictions or observables, while simultaneously generating interaction terms.

To describe gauge invariance and the consequences of requiring a lagrangian to be invariant under gauge transformations, we will begin by focusing on QED.

2.1.1   The Quantum Electrodynamics

Let us take a moment to consider the following lagrangian

$$\mathcal{L} = i\overline{\psi}\left(x\right)\slashed{\partial}\psi\left(x\right) + m\overline{\psi}\left(x\right)\psi\left(x\right), \tag{2.1}$$

where $\slashed{\partial} = \gamma^\mu \partial_\mu$. Here $\gamma^\mu \to \{\gamma^0, \gamma^1, \gamma^2, \gamma^3\}$ represent the gamma matrices, also called the Dirac matrices, and follow the anticommutation algebra $\{\gamma^\mu, \gamma^\nu\} = \gamma^\mu\gamma^\nu + \gamma^\nu\gamma^\mu$. In the QFT approach, the above lagrangian is known as the Dirac Lagrangian, which describes the physics of a free fermion $\psi\left(x\right)$ with mass m and spin-1/2[4] [2, 4]. If we demand that the fermion fields $\psi\left(x\right)$ transform under the following global $U(1)$ transformation

$$\begin{aligned}\psi\left(x\right) &\to \psi'\left(x\right) = e^{-ieQ\alpha}\psi\left(x\right), \\ \overline{\psi}\left(x\right) &\to \overline{\psi'}\left(x\right) = \overline{\psi}\left(x\right)e^{ieQ\alpha},\end{aligned} \tag{2.2}$$

where α is an arbitrary constant, e is the unit of electric charge and Q is the charge operator (i.e. $Q\psi = -\psi$), we can easily see that the lagrangian is automatically invariant. However, if the arbitrary α depends on the space-time coordinates as $\alpha \to \alpha\left(x\right)$, we obtain

---

[3]   Within QFT, these fields and potentials describe the behavior of particles.
[4]   A free fermion field refers to a fermion field that does not interact with other fields.

$$\psi\left(x\right) \rightarrow \psi'\left(x\right) = e^{-ieQ\alpha(x)}\psi\left(x\right),$$
$$\overline{\psi}\left(x\right) \rightarrow \overline{\psi'}\left(x\right) = \overline{\psi}\left(x\right)e^{ieQ\alpha(x)},$$
(2.3)

or for a infinitesimal $\alpha\left(x\right)$ we have

$$\psi\left(x\right) \rightarrow \left(1 - ieQ\alpha\left(x\right)\right)\psi\left(x\right).$$
(2.4)

By substituting the Eq. (2.3) or Eq. (2.4) in Eq. (2.1), we can verify that the lagrangian is no longer invariant under local $U(1)$ gauge transformations. To maintain invariance under local $U(1)$ gauge transformations, we must replace the partial derivative ∂_μ with the following expression

$$\partial_\mu \rightarrow D_\mu = \partial_\mu + ieA_\mu Q,$$
(2.5)

where D_μ represents the covariant derivative, and $A_\mu\left(x\right)$ denotes the electromagnetic field. In addition to introducing the covariant derivative, the field $A_\mu\left(x\right)$ must transform as

$$A_\mu\left(x\right) \rightarrow A'_\mu\left(x\right) = A_\mu + \partial_\mu\alpha\left(x\right).$$
(2.6)

The result of introducing the partial derivative from Eq. (2.5) and assuming that the electromagnetic field $A_\mu\left(x\right)$ transforms according to Eq. (2.6) is the following lagrangian

$$\mathcal{L} = -\frac{1}{4}F_{\mu\nu}\left(x\right)F^{\mu\nu}\left(x\right) + \overline{\psi}\left(x\right)\left(i\slashed{D} - m\right)\psi\left(x\right).$$
(2.7)

This new Dirac lagrangian is invariant under the $U(1)$ local gauge transformation given by Eq. (2.3) and Eq. (2.6). The first term is known as the kinetic term for the field

$A_\mu(x)$ and is defined as

$$F_{\mu\nu}(x) = \partial_\mu A_\nu(x) - \partial_\nu A_\mu(x).$$ (2.8)

This kinetic term is permitted by Lorentz invariance and is invariant under $U(1)$ local gauge transformations. It is necessary for describing the kinematics of the field $A_\mu(x)$. We observe that local gauge invariance necessitates the existence of a gauge field $A_\mu(x)$ that interacts with fermions ψ through the covariant derivative D_μ. In the language of group theory, the gauge transformation mentioned above with a scalar phase $\alpha(x)$ belongs to the unitary group $U(1)$. The full lagrangian described in Eq. (2.7) is said to possess the symmetry $U(1)_Q$ with the charge operator Q serving as the generator of the group. This invariant lagrangian describes the gauge theory known as Quantum Electrodynamics and is recognized as the quantum field theory based on the $U(1)_Q$ local gauge symmetry group. It characterizes the individual dynamics of fermions $\psi(x)$ and the electromagnetic field $A_\mu(x)$, as well as the interactions between these two fields. QED is considered one of the most accurate theories in physics as it provides a highly precise description of all electromagnetic phenomena at the quantum level.

As previously mentioned, QED is a gauge theory based on the abelian group $U(1)$, which is one of the fundamental pillars of the SM. Similarly, we can derive the description of weak interactions through the gauge invariance principle in non-abelian gauge theories, such as the Yang-Mills theories, which will be discussed in the next subsection.

2.1.2 The $SU(2)$ Yang-Mills theories

In the SM, weak interactions explain phenomena such as radioactive decays, which occurs through the exchange of highly massive bosons [5]. During the development of the SM, it was discovered that the most suitable theoretical framework to describe the phenomenology of weak interactions is the Yang-Mills gauge theories based on the $SU(2)$, following group theory principles. However, as we will discuss later, this theory has limitations because demanding gauge invariance, as done in QED, results in gauge bosons without mass. For now, we can set aside this issue and focus on demonstrating how to obtain a possible gauge theory for weak interactions. Consider the following lagrangian

$$\mathcal{L} = \overline{\psi}\left(x\right)\left(i\slashed{\partial} - m\right)\psi\left(x\right), \tag{2.9}$$

where ψ $(\overline{\psi})$ is now a column (row) vector in the isospin space. Analogously to Eq. (2.3) and Eq. (2.4), the isospin fields ψ transform as

$$\psi\left(x\right) \to \psi'\left(x\right) = e^{-ig\overrightarrow{\alpha}(x)\cdot\overrightarrow{T}}\psi\left(x\right),$$
$$\overline{\psi}\left(x\right) \to \overline{\psi'}\left(x\right) = \overline{\psi}\left(x\right)e^{ig\overrightarrow{\alpha}(x)\cdot\overrightarrow{T}}, \tag{2.10}$$

or in the infinitesimal local gauge form

$$\psi\left(x\right) \to \left[1 - ig\overrightarrow{\alpha}\left(x\right)\cdot\overrightarrow{T}\right]\psi\left(x\right), \tag{2.11}$$

where $\overrightarrow{\alpha}\left(x\right) = \left(\alpha_1\left(x\right), \alpha_2\left(x\right), \alpha_3\left(x\right)\right)$ represents arbitrary scalars in isospin space, and $\overrightarrow{T} = \left(T_1, T_2, T_3\right)$ denotes the isospin operator, with its components T_i serving as the generators of the $SU(2)$ group. It is important to note that the generators T_i do not commute and follow the following algebra

$$[T_i, T_j] = i\epsilon_{ijk}T_k. \tag{2.12}$$

Since this occurs, we say that the group is non-abelian. The generators can be defined as $T_i = \tau_i/2$, where τ_i represents the Pauli Matrices. Following the same framework discussed in Subsection 2.1.1, we can verify that for a gauge theory based on the local $SU(2)$ group, the invariant lagrangian should be

$$\mathcal{L} = -\frac{1}{4}W^a_{\mu\nu}\left(x\right)W^{\mu\nu}_a\left(x\right) + \overline{\psi}\left(x\right)\left(i\slashed{D} - m\right)\psi\left(x\right), \tag{2.13}$$

where to guarantee this invariance we replace the partial derivative ∂_μ by the following covariant derivative

$$D_\mu = \partial_\mu + igW_\mu^a T^a. \tag{2.14}$$

In this case, the gauge fields $W_\mu^a(x)$ should transform as follows

$$W_\mu^a(x) \to W_\mu'^a(x) = W_\mu^a(x) + \partial_\mu \alpha^a(x) + g\epsilon^{abc}\alpha^b(x)W_\mu^c(x). \tag{2.15}$$

The first term of the lagrangian in Eq. (2.13) is permitted by Lorentz invariance. It is essential for describing the kinematics of the gauge bosons W_μ^a, where

$$W_{\mu\nu}^a(x) = \partial_\mu W_\nu^a(x) - \partial_\nu W_\mu^a(x) - g\epsilon^{abc}W_\mu^b(x)W_\nu^c(x). \tag{2.16}$$

As mentioned earlier, a gauge model based on the $SU(2)$ group, described by the lagrangian in Eq. (2.13), is a suitable candidate for incorporating the phenomenology of weak interactions. One possibility to accommodate weak interactions within the $SU(2)$ group is to combine the isospin triplet W_μ^a to form the physical bosons $W_\mu^\pm$ and Z_μ, as follows

$$
\begin{aligned}
W_\mu^\pm &= \frac{1}{\sqrt{2}}\left(W_\mu^1 \mp iW_\mu^2\right), \\
Z_\mu &= W_\mu^3.
\end{aligned}
\tag{2.17}
$$

However, some remarks regarding this result need to be addressed. We are aware that the weak interactions require the vector bosons $W_\mu^\pm$ and Z_μ to have mass. This necessitates the inclusion of a mass term in the following form

$$\mathcal{L}_{mass}^{W_a} = M^2 W_\mu^a W_a^\mu. \tag{2.18}$$

This mass term is permitted by Lorentz invariance. However, it is not invariant under the local gauge transformations described in Eq. (2.15). On the other hand, we

know that particles that interact through weak currents must exhibit a vector-axial (V-A) interaction structure since experiments have shown the existence of a left-handed structure for charged and neutral weak currents [5–7]. This $V - A$ structure arises as a consequence of the observed parity violation in weak interactions, which is not apparent in the lagrangian given in Eq. (2.13). As we will explore in the next section, the solution to these problems lies in a unified theoretical framework known as the Electroweak Standard Model. This unified framework combines the $SU(2)$ and $U(1)$ gauge symmetries previously discussed and allows for the introduction of fermions with left chirality. This framework accurately reproduces all observations related to interactions among fundamental particles, such as the $V - L$ structure, recovers the QED, and also incorporates the generation of mass for physical bosons through a mechanism known as the Higgs mechanism.

2.2 The Standard Model Lagrangian

The SM is a gauge theory based on the $SU(3)_C \times SU(2)_L \times U(1)_Y$ gauge symmetry group. The label C indicates that the theory is based on the $SU(3)_C$ group, known as Quantum Chromodynamics (QCD), which deals with particles possessing the quantum number C, also referred to as Color Charge. The label L indicates that the theory based on the $SU(2)_L$ group is a chiral theory. This is because left-handed and right-handed fermions are treated differently under transformations of this group. The label Y in $U(1)_Y$ indicates that this group deals with fermions possessing the quantum number Y, known as Weak Hypercharge [3, 5].

As observed, each symmetry group determines the type of fundamental interaction, and the number of gauge bosons is directly related to the number of group generators[5]. In strong interactions, we have 8 bosons known as Gluons, while in electroweak interactions, we have 4 bosons named $W^{\pm}$, Z, and the photon A. As mentioned previously, since the strong sector does not break or mix with the electroweak sector, this review of the SM focuses exclusively on the Electroweak Standard Model [8–10].

The generators T_a of the weak isospin group $SU(2)_L$ satisfy the same algebra as shown in Eq. (2.12). Regarding the weak hypercharge group $U(1)_Y$, the generator is the weak hypercharge operator Y, which is related to the diagonal generator T_3 through the Gell-Mann-Nishijima relation [3]

---

[5] In gauge theories based on $SU(N)$ and $U(N)$ groups, the number of generators is $N^2 - 1$ and N^2, respectively.

$$Q = T_3 + \frac{Y}{2}, \tag{2.19}$$

where Q represents the electric charge operator. We are aware of the existence of 12 fundamental fermions in nature: three charged leptons e, μ, τ, three neutrinos ν_e, ν_μ, ν_τ, and six quarks u, d, c, s, t, b [11]. We can classify the quarks into two types: up-type quarks (u, c, t) and down-type quarks (d, s, b). Since the SM is a chiral theory, these fermions transform differently under transformations of the $SU(2)_L$ group: left-handed fermions ψ_L transform as doublets, while right-handed fermions ψ_R transform as singlets. As the SM is a phenomenologically constructed theoretical framework, it is necessary to reproduce all experimental observations concerning fundamental particles. To achieve this, we must organize the matter content as follows

$$L_{aL} = \begin{pmatrix} \nu_a \\ l_a \end{pmatrix}_L \sim (\underline{1}, \underline{2}, -1), \quad l_R^a \sim (\underline{1}, \underline{1}, -2), \tag{2.20}$$

where a is a label used to indicate the generation of the neutrino ν_a and charged lepton l_a with $a = e, \mu, \tau$ corresponding to the first, second, and third generations, respectively[6]. In the quark sector, we have

$$Q_{aL} = \begin{pmatrix} u_a \\ d_a \end{pmatrix}_L \sim (\underline{3}, \underline{2}, 1/3), \quad u_R^a \sim (\underline{3}, \underline{1}, 4/3), \quad d_R^a \sim (\underline{3}, \underline{1}, -2/3). \tag{2.21}$$

In this case, the label a denotes the family number for the up- and down-type quarks, where $a = u, c, t$ in the first component, and $a = d, s, b$ in the second component. The notation $\sim \left(\underline{g_1}, \underline{g_2}, g_3 \right)$ indicates how the different fields transform under each SM group: $\underline{g_1} = \underline{1}(\underline{3})$ implies that the field in question transforms as a singlet (triplet) under $SU(3)_C$, $\underline{g_2} = \underline{1}(\underline{2})$ implies that the field transforms as a singlet (doublet) of $SU(2)_L$, and g_3 represents the weak hypercharge value Y of the field, which can be determined using Eq. (2.19).

---

[6]   The SM fermions can be classified into generations or families based on their mass (in increasing order).

Thus, for example, if $a = e$ in the lepton doublet, $L_{eL} \sim (\underline{1}, \underline{2}, -1)$ is a vector whose components are leptons of the first family (neutrino ν_e in the first row and electron e in the second row) that transform as a singlet of $SU(3)_C$, a doublet of $SU(2)_L$ with hypercharge $Y = -1$.

The left-handed and right-handed chiralities of a fermion field ψ are defined as

$$\psi_{L,R} = \frac{1}{2} \left(1 \mp \gamma^5 \right) \psi, \tag{2.22}$$

where $\gamma^5 = i\gamma^0\gamma^1\gamma^2\gamma^3$. The gamma matrices γ^μ satisfy the following anti-commutative algebra $[\gamma^\mu, \gamma^\nu]_+ = 2g^{\mu\nu}$ where $g^{\mu\nu}$ is the Minkowski metric tensor with $\mu = 0, 1, 2, 3$. Table 1 shows the quantum numbers of the fields using the Eq. (2.19).

Table 1 – Quantum numbers of fermions f in the SM.

Fermion	T_{3f}	Y_f	Q_f
l_{aL}	-1/2	-1	-1
l_{aR}	0	-2	-1
ν_{aL}	1/2	-1	0
u_{aL}	1/2	1/3	2/3
d_{aL}	-1/2	1/3	-1/3
u_{aR}	0	4/3	2/3
d_{aR}	0	-2/3	-1/3

To explain the various types of interactions in detail, we have divided the SM lagrangian into sectors. Taking everything into consideration, the SM lagrangian can be written in the following form

$$\mathcal{L}_{SM} = \mathcal{L}_{Fermions} + \mathcal{L}_{Gauge} + \mathcal{L}_{Scalar} + \mathcal{L}_{Yukawa}. \tag{2.23}$$

The above lagrangian is Lorentz invariant, invariant under $SU(2)_L \times U(1)_Y$ transformations, and renormalizable. Each sector of the lagrangian will be explained in detail

in the next subsections.

2.2.1 The Fermion Sector

The lagrangian that describes the kinematics and interactions between fermions and gauge bosons is as follows

$$\mathcal{L}_{Fermions} = i\overline{L_{aL}}\slashed{D}L_{aL} + i\overline{Q_{aL}}\slashed{D}Q_{aL} + i\overline{l_{aR}}\slashed{D}l_{aR} + i\overline{u_{aR}}\slashed{D}u_{aR} + i\overline{d_{aR}}\slashed{D}d_{aR}. \tag{2.24}$$

The Einstein summation convention has been used. As discussed in Subsection 2.1.1 and Subsection 2.1.2, in order to ensure invariance, we need to replace the partial derivative ∂_μ with the covariant derivative D_μ. Therefore, using Eq. (2.5) and Eq. (2.14) and taking into account that covariant derivatives will take on different forms depending on whether they are applied to left-handed or right-handed fields, the covariant derivatives for left-handed and right-handed fermions are respectively

$$\slashed{D} = \slashed{\partial} + i\frac{g}{2}\tau^a\slashed{W}^a + ig'\slashed{B}\frac{Y}{2}, \tag{2.25}$$

$$\slashed{D} = \slashed{\partial} + ig'\slashed{B}\frac{Y}{2}, \tag{2.26}$$

where τ^a represents the Pauli matrices, Y is the weak hypercharge operator, and g and g' are the coupling constants for theories based on the $SU(2)_L$ and $U(1)_Y$ groups, respectively. We observe that the substitution of the partial derivatives introduces new boson fields W_μ^a and B_μ associated with the $SU(2)_L$ and $U(1)_Y$ groups, respectively. These bosons are known as unphysical boson states. Furthermore, to proceed with the construction of a gauge theory, which requires invariance under local gauge transformations, the fermions and bosons must transform as follows

$$SU(2)_L \times U(1)_Y \rightarrow \begin{cases} \Psi(x)_L \rightarrow \Psi'(x)_L = e^{-igT^a\alpha_a(x)-ig'\frac{Y}{2}\eta(x)}\Psi(x)_L, \\ \psi(x)_R \rightarrow \psi'(x)_R = e^{-ig'\frac{Y}{2}\eta(x)}\psi(x)_R, \\ W^a_\mu(x) \rightarrow W'^a_\mu(x) = W^a_\mu(x) + \partial_\mu\alpha^a(x) + g\epsilon^{abc}\alpha_b(x)W_{c\mu}(x), \\ B_\mu \rightarrow B'_\mu = B_\mu + \partial_\mu\eta(x), \end{cases}$$

$$(2.27)$$

where $\eta(x)$ and $\alpha(x)$ are arbitrary parameters, and ϵ^{abc} is a totally antisymmetric tensor. Each line in Eq. (2.27) shows how the SM fields transform under transformations of the $SU(2)_L \times U(1)_Y$ group. The first and second lines represent the transformations for the left-handed doublets $\Psi(x)_L$ and the right-handed singlets $\psi(x)_R$, respectively, where $\Psi(x)_L$ includes $L(x)_L$ and $Q(x)_L$, while $\psi(x)_R$ includes $l(x)_R$, $u(x)_R$, and $d(x)_R$. The third and fourth lines show the transformations of the unphysical boson states W^a_μ and B_μ associated with the $SU(2)_L$ (non-abelian) and $U(1)_Y$ (abelian) groups, respectively.

The process of demanding gauge invariance results in the emergence of interaction terms between the fermions of the theory and the gauge bosons[7]. Therefore, using Eq. (2.25), Eq. (2.26), and the values of the weak hypercharges of the fermions shown in Table 1, we can derive the following interaction lagrangians between fermions and bosons in the physical basis

$$\mathcal{L}^{CC}_{Fermions} = -\frac{g}{2\sqrt{2}}\left(j^\mu_{W,l} + j^\mu_{W,Q}\right)W_\mu + h.c., \qquad (2.28)$$

$$\mathcal{L}^{NC}_{Fermions} = -e\left(j^\mu_{A,l} + j^\mu_{A,Q}\right)A_\mu - \frac{g}{2cos\theta_W}\left(j^\mu_{Z,l} + j^\mu_{Z,Q}\right)Z_\mu, \qquad (2.29)$$

where $h.c.$ denotes "hermitian conjugate"[8]. The lagrangian shown in Eq. (2.28) is referred to as the charged current lagrangian since it describes the coupling between the charged currents $j^\mu_{W,l}$ (for charged leptons l) and $j^\mu_{W,Q}$ (for quarks Q) with the electrically

---

[7] In this subsection, we will only discuss the interaction terms resulting from the requirement of gauge invariance in the SM; hence, the kinetic terms for fermions will be omitted.

[8] "+h.c."is an abbreviation for "plus the Hermitian conjugate". It indicates that there are additional terms in the lagrangian that are the Hermitian Conjugates of all the preceding terms. This inclusion ensures that the lagrangian remains hermitian.

charged boson $W^{\pm}$. On the other hand, the lagrangian in Eq. (2.29) is known as the neutral current lagrangian as it couples the neutral currents $j^{\mu}_{A,f}$ and $j^{\mu}_{Z,f}$ (for all fermions f) with the electrically neutral bosons A (photon) and Z, respectively. It is important to note that the fields W_{μ} and Z_{μ} represent physical states and are related to the unphysical states W^a_{μ} and B_{μ} as follows

$$W^{\mu} = \frac{W^{\mu}_1 - iW^{\mu}_2}{\sqrt{2}}, \tag{2.30}$$

$$\begin{pmatrix} A^{\mu} \\ Z^{\mu} \end{pmatrix} = \begin{pmatrix} cos\theta_W & sin\theta_W \\ -sin\theta_W & cos\theta_W \end{pmatrix} \begin{pmatrix} B^{\mu} \\ W^{\mu}_3 \end{pmatrix}, \tag{2.31}$$

where the angle θ_W that relates the physical states (A, Z) and unphysical states (B, W^3) is known as the Weinberg angle or electroweak mixing angle and has a value of $\sin^2\theta_W = 0.23122(4)$ [12]. On the other hand, the charged currents that couple the $W^{\pm}$ boson with the charged leptons and quarks that appear in Eq. (2.28) are defined as follows

$$j^{\mu}_{W,l} = 2\overline{\nu_{lL}}\gamma^{\mu}l_L = \overline{\nu_l}\gamma^{\mu}\left(1 - \gamma^5\right)l, \tag{2.32}$$

$$j^{\mu}_{W,Q} = 2\overline{u_L}\gamma^{\mu}d_L = \overline{u}\gamma^{\mu}\left(1 - \gamma^5\right)d. \tag{2.33}$$

In the case of neutral currents that appear in Eq. (2.29), the currents that couple leptons l and quarks Q to the Z boson have the following form

$$\begin{aligned} j^{\mu}_{Z,l} &= 2\left(g^{\nu}_L\overline{\nu_{lL}}\gamma^{\mu}\nu_{lL} + g^l_L\overline{l_L}\gamma^{\mu}l_L + g^l_R\overline{l_R}\gamma^{\mu}l_R\right) \\ &= \overline{\nu_l}\gamma^{\mu}\left(g^{\nu}_V - g^{\nu}_A\gamma^5\right)\nu_l + \overline{l}\gamma^{\mu}\left(g^l_V - g^l_A\gamma^5\right)l, \end{aligned} \tag{2.34}$$

$$\begin{aligned} j^{\mu}_{Z,Q} &= 2\left(g^U_L\overline{u_L}\gamma^{\mu}u_L + g^U_R\overline{u_R}\gamma^{\mu}u_R + g^D_L\overline{d_L}\gamma^{\mu}d_L + g^D_R\overline{d_R}\gamma^{\mu}d_R\right) \\ &= \overline{u}\gamma^{\mu}\left(g^U_V - g^U_A\gamma^5\right)u + \overline{d}\gamma^{\mu}\left(g^D_V - g^D_A\gamma^5\right)d, \end{aligned} \tag{2.35}$$

while, as described in Subsection 2.1.1, the lagrangian of QED retains its usual form

$$j^{\mu}_{A,f} = Q_f \overline{f} \gamma^{\mu} f, \tag{2.36}$$

where Q_f represents the electric charge of the fermion f. It can be observed that we recover the same electromagnetic current that arises when substituting Eq. (2.5) into the second term of Eq. (2.7). By examining Eq. (2.32), Eq. (2.33), Eq. (2.34), and Eq. (2.35), we can observe that the currents associated with the $W^{\pm}$ and Z bosons, as present in the charged and neutral current lagrangian, exhibit the $(V - A)$ interaction required to accurately reproduce the observed parity violation in weak interactions. The specific values of the couplings $g^f_{L,R}$ and $g^f_{V,A}$ can be found in Table 2.

Table 2 – Coupling constants for fermions f in the SM.

Fermions	g^f_L	g^f_R	g^f_V	g^f_A
ν_l	$\frac{1}{2}$	0	$\frac{1}{2}$	$\frac{1}{2}$
l	$-\frac{1}{2} + sin^2\theta_W$	$sin^2\theta_W$	$-\frac{1}{2} + 2sin^2\theta_W$	$-\frac{1}{2}$
u-type	$\frac{1}{2} - \frac{2}{3}sin^2\theta_W$	$-\frac{2}{3}sin^2\theta_W$	$\frac{1}{2} - \frac{4}{3}sin^2\theta_W$	$\frac{1}{2}$
d-type	$-\frac{1}{2} + \frac{1}{3}sin^2\theta_W$	$\frac{1}{3}sin^2\theta_W$	$-\frac{1}{2} + \frac{2}{3}sin^2\theta_W$	$-\frac{1}{2}$

2.2.2 The Gauge Sector

We have observed that the lagrangian presented in Eq. (2.24) describes the kinematics of fermions and their interactions with bosons. However, the SM lagrangian must also include a term that describes free bosons, as well as their interactions with each other [2]. Furthermore, it should remain invariant under Lorentz and gauge transformations. These requirements are fulfilled by the following lagrangian

$$\mathcal{L}_{Gauge} = -\frac{1}{4}B_{\mu\nu}(x)B^{\mu\nu}(x) - \frac{1}{4}W^a_{\mu\nu}(x)W^{\mu\nu}_a(x), \tag{2.37}$$

where

$$B_{\mu\nu} = \partial_\mu B_\nu - \partial_\nu B_\mu, \tag{2.38}$$

$$W^a_{\mu\nu} = \partial_\mu W^a_\nu - \partial_\nu W^a_\mu - g\epsilon^{abc}W^b_\mu W^c_\nu. \tag{2.39}$$

The invariance of Eq. (2.37) under $SU(2)_L \times U(1)_Y$ transformations is guaranteed if the bosons transform according to Eq. (2.27). By substituting Eq. (2.30) and Eq. (2.31) into Eq. (2.37), we obtain the lagrangian in terms of the physical states

$$
\begin{aligned}
\mathcal{L}_{Gauge} = & -\frac{1}{2}F^\dagger_{W\mu\nu}F^{\mu\nu}_W - \frac{1}{4}F_{Z\mu\nu}F^{\mu\nu}_Z - \frac{1}{4}F_{\mu\nu}F^{\mu\nu} \\
& + igcos\theta_W \left(F^{\mu\nu}_W Z_\mu W^\dagger_\nu - F^\dagger_{W\mu\nu}Z^\mu W^\nu + F^{\mu\nu}_Z W^\dagger_\mu W_\nu \right) \\
& + ie \left(F^{\mu\nu}_W A_\mu W^\dagger_\nu - F^\dagger_{W\mu\nu}A^\mu W^\nu + F^{\mu\nu}W^\dagger_\mu W_\nu \right) \\
& + (gcos\theta_W)^2 \left[(W_\mu Z^\mu)(W^\dagger_\nu Z^\nu) - (W^\mu W^\dagger_\mu)(Z^\nu Z_\nu) \right] \\
& + e^2 \left[(W_\mu A^\mu)(W^\dagger_\nu A^\nu) - (W^\mu W^\dagger_\mu)(A^\nu A_\nu) \right] \\
& + egcos\theta_W \left[(W_\mu Z^\mu)(W^\dagger_\nu A^\nu) + (W^\dagger_\mu Z^\mu)(W_\nu A^\nu) - 2(W^\mu W^\dagger_\mu)(Z_\nu A^\nu) \right] \\
& + \frac{g^2}{2} \left[(W_\mu W^\mu)(W^\dagger_\nu W^{\dagger\nu}) - (W^\dagger_\mu W^\mu)^2 \right],
\end{aligned}
\tag{2.40}
$$

where

$$F_{\mu\nu} = \partial_\mu A_\nu - \partial_\nu A_\mu, \tag{2.41}$$

$$F_{W\mu\nu} = \partial_\mu W_\nu - \partial_\nu W_\mu, \tag{2.42}$$

$$F_{Z\mu\nu} = \partial_\mu Z_\nu - \partial_\nu Z_\mu. \tag{2.43}$$

The first, second, and third terms of the first line in Eq. (2.40) describe the free bosons $W^\pm$, Z, and the photon A, respectively. The remaining terms describe the interactions and self-interactions between them. As discussed in Subsection 2.1.2, these

self-interaction terms are a direct consequence of the non-abelian property of the $SU(2)_L$ group. Since the $U(1)_Y$ group is abelian, there are no self-interaction terms for the bosons Z_μ and A_μ.

2.2.3 The Scalar Sector

So far, we have presented lagrangians that describe the kinematics of fermions and bosons, as well as their interactions. However, no mass terms have been introduced in the following form

$$m\overline{\psi}\psi = m\left(\overline{\psi_L}\psi_R + \overline{\psi_R}\psi_L\right),$$
(2.44)

$$M_W^2 W_\mu^\dagger W^\mu + M_Z^2 Z_\mu Z^\mu.$$
(2.45)

This is because, as discussed throughout this chapter, in order to reproduce all the particle physics phenomenology, the group that accommodates weak and electromagnetic interactions is the $SU(2)_L \times U(1)_Y$ group. The SM theory is based on this chiral symmetry group, with left-handed and right-handed fermions transforming differently: left-handed fermions transform as doublets, while right-handed fermions transform as singlets. If we substitute the transformations given by Eq. (2.27) into Eq. (2.44) and Eq. (2.45), we can verify that mass terms for fermions and bosons explicitly violate the gauge symmetry. Therefore, mass terms are forbidden if we consider transformations under $SU(2)_L \times U(1)_Y$.

To obtain a renormalizable theory that allows for the introduction of mass terms for fermions and bosons, we need a mechanism in which the original symmetry of the SM is broken, resulting in the generation of mass terms for fermions and bosons (except for the photon). In the SM, the mechanism that satisfies these requirements is known as the Brout–Englert–Higgs Mechanism[9]. The Higgs mechanism is a physical mechanism in which mass terms for fermions and bosons are generated through a process known as Spontaneous Symmetry Breaking (SSB). Proposed in the 1960s, this mechanism predicts the existence of a new scalar (spin-0) boson called the Higgs Boson. On July 4, 2012,

---

[9] Throughout this thesis, we will refer to this mechanism as the Higgs Mechanism, as it is the most commonly used term in the literature.

the CMS and ATLAS collaborations confirmed the detection of a scalar particle that exhibited properties consistent with those expected for the Higgs boson [13, 14]. This particle represented a significant confirmation of the SM and led to Peter Higgs and François Englert being awarded the Nobel Prize in Physics in 2013. In this subsection, we will qualitatively and quantitatively explain the Higgs mechanism and its connection to SSB.

We know that the SM lagrangian must be constructed to be symmetric under transformations of the $SU(2)_L \times U(1)_Y$ gauge group. Let's assume that this lagrangian has degenerate minimum energy states. If we choose one of these minimum energy states to be the vacuum state and find that the vacuum state does not possess the original symmetry of the lagrangian, we say that the symmetry has been spontaneously broken. The vacuum state should be electrically neutral and invariant under transformations of the electromagnetic group $U(1)_Q$, as discussed in Subsection 2.1.1. As we will explore in this subsection, the SSB in the SM occurs as $SU(2)_Y \times U(1)_Y \rightarrow U(1)_Q$.

To construct the Higgs mechanism, we will introduce the following scalar doublet, which is invariant under Lorentz transformations and has a non-zero vacuum expectation value (VEV) [2]

$$\Phi(x) = \begin{pmatrix} \phi^+(x) \\ \phi^0(x) \end{pmatrix} \sim (\underline{1}, \underline{2}, 1), \tag{2.46}$$

where $\phi^+(x)$ and $\phi^0(x)$ are electrically charged and neutral scalar fields, respectively. The scalar lagrangian that enables SSB is

$$\mathcal{L}_{Scalar} = [D^\mu \Phi(x)]^\dagger D_\mu \Phi(x) - V(x), \tag{2.47}$$

where the scalar potential $V(x)$ is defined as

$$V(x) = \mu^2 \Phi(x)^\dagger \Phi(x) + \lambda \left[\Phi(x)^\dagger \Phi(x) \right]^2, \tag{2.48}$$

where μ and λ are, initially, arbitrary parameters. The lagrangian in Eq. (2.47) is

(a) $\mu^2 > 0$ (b) $\mu^2 < 0$
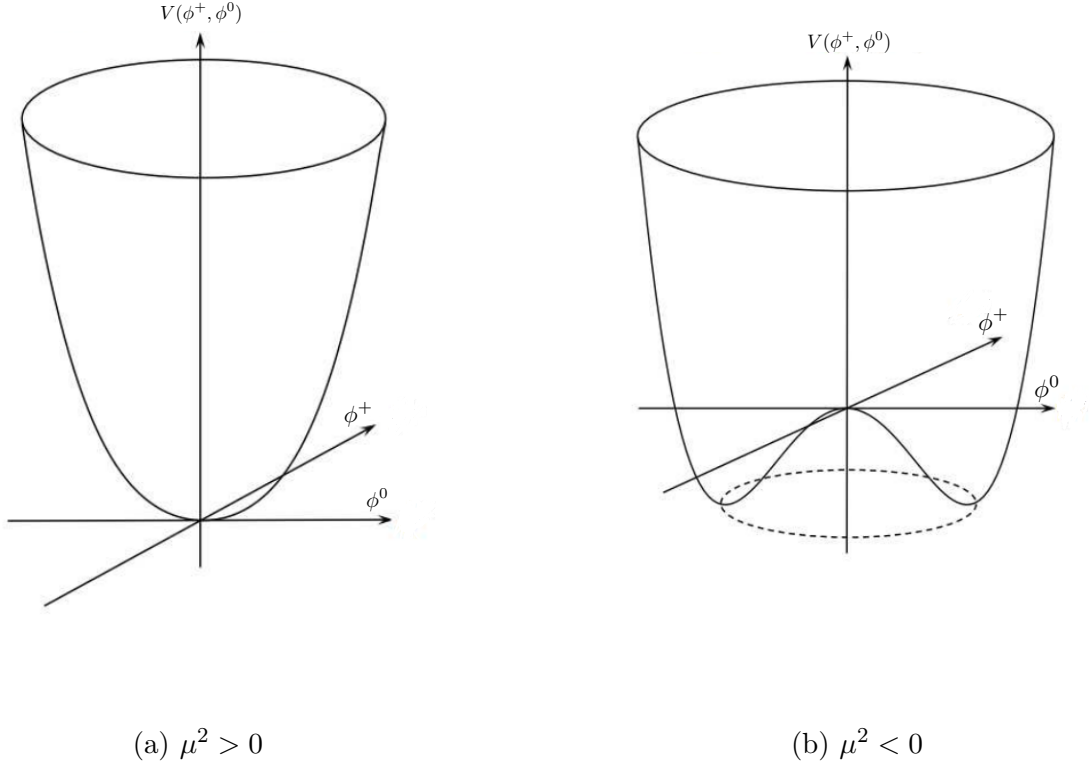
Figure 1 – Potential $V(x)$ for the cases (a) $\mu^2 > 0$ and (b) $\mu^2 < 0$

invariant under $SU(2)_Y \times U(1)_Y$ transformations as long as $\Phi(x)$ transforms as follows

$$\Phi(x) \rightarrow \Phi'(x) = e^{-igT^a\alpha_a(x) - ig'\frac{Y}{2}\eta(x)}\Phi(x). \tag{2.49}$$

Now we will analyze the system described by the lagrangian in Eq. (2.47) in its lowest energy state, where the energy corresponds to the constant value Φ_0 that minimizes the potential V. The parameters μ and λ in the potential $V(x)$ must satisfy certain physical requirements. The parameter λ must be positive for $V(x)$ to be bounded from below, while the parameter μ can have positive or negative values, as illustrated in Figure 1. As shown in the figure, when $\mu^2 > 0$, there is only one minimal energy state, given by $\Phi_0 = (0,0)^T$, and SSB does not occur. As mentioned before, SSB is only relevant in theories with degenerate minimum energy states[10]. However, as shown in Figure 1, the scenario when $\mu^2 < 0$ is ideal for SSB, as there exists an infinite set of minimum energy states. The potential $V(x)$ can be written as follows

---

[10] This can be trivially checked by performing infinitesimal transformations using Eq. (2.49) since the minimal energy state with $\Phi_0 = \begin{pmatrix} 0 & 0 \end{pmatrix}^T$ is an eigenstate of the generators $G = \{T_1, T_2, T_3, Y\}$.

$$V\left(x\right) = \lambda\left[\Phi\left(x\right)^\dagger \Phi\left(x\right) + \frac{\mu^2}{2\lambda}\right]^2 - \lambda\left(\frac{\mu^2}{2\lambda}\right)^2. \tag{2.50}$$

We can observe that the potential has an infinite set of minimum energy states for a specific constant value of the Higgs field, given by

$$\Phi_0 = \begin{pmatrix} \phi_0^+ \\ \phi_0^0 \end{pmatrix} \quad \text{with} \quad \Phi_0^\dagger \Phi_0 = -\frac{\mu^2}{2\lambda}. \tag{2.51}$$

The vacuum state corresponds to one of those minimum energy states (represented by the dashed circle in Figure 1). Therefore, the minimum energy state is not unique, and SSB can occur for arbitrary values of ϕ_0^+ and ϕ_0^0 that satisfy the condition given by Eq. (2.51). We will choose the following minimum energy state as the vacuum state

$$\Phi_0 = \begin{pmatrix} \phi_0^+ \\ \phi_0^0 \end{pmatrix} = \frac{1}{\sqrt{2}} \begin{pmatrix} 0 \\ v \end{pmatrix}, \tag{2.52}$$

where v is known as the VEV of the Higgs Field and is defined as

$$v = \sqrt{-\frac{\mu^2}{\lambda}}. \tag{2.53}$$

We can easily verify that the vacuum state of Eq. (2.52) is no longer an eigenstate of the generators $G = \{T_1, T_2, T_3, Y\}$. Therefore, we say that the vacuum state is no longer invariant under transformations of the $SU(2)_L \times U(1)_Y$ group. However, we can also verify that the vacuum state is an eigenstate of the generator Q of the electromagnetic group given by Eq. (2.19). This confirms that the group $SU(2)_L \times U(1)_Y$ has been broken to $U(1)_Q$, guaranteeing the conservation of a quantity (electric charge) as well as the existence of a massless boson associated with the $U(1)_Q$ theory, identified as a photon.

Once SSB has occurred, we can analyze perturbations around the vacuum state of the theory. Perturbations of the field Φ can be obtained by considering perturbations around the vacuum state Φ_0 as follows

$$\Phi(x) = \frac{1}{\sqrt{2}} \begin{pmatrix} \phi_1(x) + i\phi_2(x) \\ v + h(x) + i\phi_3(x) \end{pmatrix}, \tag{2.54}$$

where the VEVs for the fields are $<\phi_1>_0 = <\phi_2>_0 = <\phi_3>_0 = <h>_0 = 0$, ensuring that $<\Phi>_0 = \Phi_0$. Therefore, we can say that $\Phi(x)$ has a non-zero VEV, as required. It is convenient to write the field $\Phi(x)$ as follows[11].

$$\Phi(x) = \frac{1}{\sqrt{2}} e^{\frac{i}{v}\phi(x)_a T^a} \begin{pmatrix} 0 \\ v + h(x) \end{pmatrix}. \tag{2.55}$$

The fields $\phi_a(x)$ correspond to massless scalar bosons known as Nambu-Goldstone bosons[12]. However, for simplicity, we aim to obtain a theory without Goldstone bosons. To achieve this, we can perform a rotation that eliminates the Goldstone bosons using the parameters of the gauge transformation $\alpha_a(x)$ and $\eta(x)$. Thus, to obtain a theory without Goldstone bosons, we can choose $\alpha_a(x) = -\phi_a/gv$ and $\eta(x) = 0$ in the transformation given by Eq. (2.49). This particular gauge choice is known as the Unitary Gauge since it allows only physical states to appear in the theory. Substituting Eq. (2.55) into Eq. (2.49) and using the unitary gauge, we obtain

$$\Phi'(x) = \frac{1}{\sqrt{2}} \begin{pmatrix} 0 \\ v + h(x) \end{pmatrix}. \tag{2.56}$$

Taking the above equation into account, we can express the lagrangian from Eq. (2.47) as follows

---

[11] The first-order approximation of Eq. (2.55) leads to Eq. (2.54). Therefore, the field given by Eq. (2.55) is more general and satisfies Eq. (2.51).

[12] Nambu-Goldstone bosons are bosons that arise in theories with spontaneous breaking of continuous symmetries.

$$\mathcal{L}_{Scalar} = \frac{1}{2}\left(\partial_\mu h\right)\left(\partial^\mu h\right) - \lambda v^2 h^2 - \lambda v h^3 - \frac{\lambda}{4}h^4$$
$$+ \frac{g^2 v^2}{4}W_\mu^\dagger W^\mu + \frac{g^2 v^2}{8c_W^2}Z_\mu Z^\mu \qquad (2.57)$$
$$+ \frac{g^2 v}{4}W_\mu^\dagger W^\mu h + \frac{g^2 v}{4c_W^2}Z_\mu Z^\mu h + \frac{g^2}{4}W_\mu^\dagger W^\mu h^2 + \frac{g^2 v}{8c_W^2}Z_\mu Z^\mu h^2.$$

We can observe that the Higgs mechanism generates a new massive scalar boson, denoted as $h(x)$, which is known as the Higgs boson. The kinematics, mass term, and self-interactions of the Higgs boson are described by the first line of the previous lagrangian. Another important result to highlight is the emergence of mass terms for the bosons $W^\pm$ and Z, while, as expected, no mass term appears for the photon A. The last line of the lagrangian depicts the interaction between the Higgs boson and the $W^\pm$ and Z bosons. By examining the quadratic terms, which correspond to mass terms, we can identify the following masses for the bosons [3]

$$m_h = \sqrt{2\lambda v^2} = \sqrt{-2v^2},$$
$$m_W = \frac{gv}{2}, \qquad (2.58)$$
$$m_Z = \frac{gv}{2c_W}.$$

In the SM, the parameter μ is a free parameter that is directly related to the mass of the Higgs boson, denoted as m_h (which is not predicted by the theory). Thus, the SM predicts the existence of a massive scalar boson h with an undetermined mass m_h that must be determined experimentally. On July 4, 2012, the ATLAS and CMS collaborations announced the discovery of a massive scalar particle that is compatible with the properties of the Higgs boson. The reported mass was 126.0±0.4(stat)±0.4 (sys) GeV by ATLAS and 125.3±0.4(stat.)±0.5 (sys) GeV by CMS [12–14].

Finally, unlike the Higgs boson, the SM predicts specific masses for the $W^\pm$ and Z bosons, which are $m_W = 77.5$ GeV and $m_Z = 88.4$ GeV, respectively. These predicted values are very close to the experimentally measured values of $m_W = 80.398 \pm 0.023$ GeV and $m_Z = 91.1876 \pm 0.0021$ GeV reported to date [12].

2.2.4 The Yukawa Sector

As we saw in the previous subsection, the Higgs mechanism allowed us to generate masses for the bosons in the SM (excluding the photon), resulting in the emergence of a new massive scalar boson known as the Higgs Boson. This was made possible by substituting the Higgs field $\Phi(x)$ using the unitary gauge. In this subsection, we will explore how the SM fermions acquire mass through their interaction with the Higgs field $\Phi(x)$. Consider the following lagrangian

$$\mathcal{L}_{Yukawa} = -Y''^l_{\alpha\beta}\overline{L'_{\alpha L}}\Phi l'_{\beta R} - Y'^D_{\alpha\beta}\overline{Q'_{\alpha L}}\Phi q'^D_{\beta R} - Y'^U_{\alpha\beta}\overline{Q'_{\alpha L}}\widetilde{\Phi}q'^U_{\beta R} + h.c., \qquad (2.59)$$

where Y'^f are matrices known as Yukawa matrices of dimension 3×3 for fermions f[13]. Leptons L'_L and l'_R are shown in Eq. (2.20), while quarks Q'_L and $q'^{(U,D)}_{L,R}$ are shown in Eq. (2.21). To maintain gauge invariance, we use $\widetilde{\Phi}(x)$ defined as $\widetilde{\Phi}(x) = i\tau_2\Phi^*(x)$. The lagrangian presented above is known as the Yukawa Lagrangian and describes the interaction between the scalar field $\Phi(x)$ and fermions f. By substituting the field $\Phi(x)$ in the unitary gauge into the lagrangian from Eq. (2.59), we obtain the following expression

$$\mathcal{L}_{Yukawa} = -\frac{(v+h)}{\sqrt{2}}\left(\overline{l'_L}Y'^l l'_R + \overline{q'^U_L}Y'^U q'^U_R + \overline{q'^D_L}Y'^D q'^D_R\right) + h.c., \qquad (2.60)$$

where we have defined

$$l'_{L,R} = \begin{pmatrix} l'_e \\ l'_\mu \\ l'_\tau \end{pmatrix}_{L,R} \qquad q'^U_{L,R} = \begin{pmatrix} u' \\ c' \\ t' \end{pmatrix}_{L,R} \qquad q'^D_{L,R} = \begin{pmatrix} d' \\ s' \\ b' \end{pmatrix}_{L,R}. \qquad (2.61)$$

Now we are going to diagonalize the matrices Y'^f through the following biunitary transformations

---

[13] The prime symbol ($'$) is used to indicate fermionic fields without defined mass

$$Y^l = V_L^{l\dagger} Y'^l V_R^l \quad where \quad Y_{\alpha\beta}^l = y_\alpha^l \delta_{\alpha\beta},$$
$$Y^U = V_L^{U\dagger} Y'^U V_R^U \quad where \quad Y_{\alpha\beta}^U = y_\alpha^U \delta_{\alpha\beta}, \tag{2.62}$$
$$Y^D = V_L^{D\dagger} Y'^D V_R^D \quad where \quad Y_{\alpha\beta}^D = y_\alpha^D \delta_{\alpha\beta}.$$

Substituting the above transformations into Eq. (2.60), we obtain

$$\mathcal{L}_{Yukawa} = -\frac{(v+h)}{\sqrt{2}} \left(\overline{l_L} Y^l l_R + \overline{q_L^U} Y^U q_R^U + \overline{q_L^D} Y^D q_R^D \right) + h.c., \tag{2.63}$$

where

$$l'_{L,R} = V_{L,R}^l l_{L,R} \quad q'^U_{L,R} = V_{L,R}^U q_{L,R}^U \quad q'^D_{L,R} = V_{L,R}^D q_{L,R}^D. \tag{2.64}$$

The fields $l_{L,R}$ and $q_{L,R}^{(U,D)}$ represent the left- and right-handed components of fermions in the mass eigenstate. By considering equations Eq. (2.22) and Eq. (2.62), the lagrangian in Eq. (2.63) can be expressed as follows

$$\mathcal{L}_{Yukawa} = -m_\alpha^l \overline{l_\alpha} l_\alpha - m_\alpha^U \overline{u_\alpha} u_\alpha - m_\alpha^D \overline{d_\alpha} d_\alpha - \frac{m_\alpha^l}{v} \overline{l_\alpha} l_\alpha h - \frac{m_\alpha^U}{v} \overline{u_\alpha} u_\alpha h - \frac{m_\alpha^D}{v} \overline{d_\alpha} d_\alpha h, \tag{2.65}$$

where

$$m_\alpha^l = \frac{y_\alpha^l v}{\sqrt{2}}, \quad m_\alpha^U = \frac{y_\alpha^U v}{\sqrt{2}}, \quad m_\alpha^D = \frac{y_\alpha^D v}{\sqrt{2}}. \tag{2.66}$$

Here, the parameters y_α^l and $y_\alpha^{U,D}$ are free parameters that must be measured experimentally. The first three terms of Eq. (2.65) are mass terms of the form $m\overline{\psi}\psi$ for charged leptons, up-type quarks, and down-type quarks, while the last three terms represent the interaction between fermions and the Higgs boson. We can see two important

results here: In the lagrangian, mass terms for fermions appeared after interacting with the Higgs field, and, in turn, terms representing interactions between fermions and the Higgs boson appeared, whose interaction is proportional to their mass m_f.

It is possible to derive a third important result: since flavor eigenstates are not equal to mass eigenstates in the quark sector[14], we will examine the effects of substituting the flavor eigenstates given by Eq. (2.64) in the fermion sector. The Eq. (2.35) and Eq. (2.36) remain unchanged upon substituting Eq. (2.64) as the matrices $V_{L,R}^l$ are unitary. However, the charged currents for the quarks are modified. Substituting Eq. (2.64) into Eq. (2.33), we obtain

$$j_{W,Q}^\mu = 2\overline{q_L^{\prime U}}\gamma^\mu q_L^{\prime D} = 2\overline{q_L^U}\gamma^\mu V_{CKM} q_L^D, \tag{2.67}$$

where $V_{CKM} = V_L^{U\dagger} V_L^D$ is known as the Cabibbo-Kobayashi-Maskawa (CKM) matrix. Using the standard parameterization, we can express V_{CKM} as follows [12]

$$V_{CMK} = \begin{pmatrix} s_{12}c_{13} & s_{12}c_{13} & s_{13}e^{-i\delta} \\ -s_{12}c_{23} - c_{12}s_{23}s_{13}e^{i\delta} & c_{12}c_{23} - s_{12}s_{23}s_{13}e^{i\delta} & s_{23}c_{13} \\ s_{12}s_{23} - c_{12}c_{23}s_{13}e^{i\delta} & -c_{12}s_{23} - s_{12}c_{23}e^{i\delta} & c_{23}c_{13} \end{pmatrix}, \tag{2.68}$$

where we use the notation $c_{ij} = cos\theta_{ij}$ and $s_{ij} = sin\theta_{ij}$. The parameters c_{ij}, s_{ij}, and δ are free parameters that are determined through processes involving quarks.

As mentioned in the introduction of this work, the main focus of this thesis is to study new physics beyond the standard model within the context of collider physics. The most common approach to studying BSM physics is to extend the symmetry group of the standard model, $SU(2)_L \times U(1)_Y$, to a larger symmetry group G. Through one or several processes of spontaneous symmetry breaking, we can restore the standard model symmetry group and recover all the physics discussed in this chapter, i.e., $G \to SU(2)_L \times U(1)_Y \to U(1)_Q$. Therefore, it was necessary to revise the standard model, as the same process carried out in this chapter to obtain interactions from the lagrangian

---

[14] Inside the SM, the neutrino fields transform under the same matrix as the charged leptons

of Eq. (2.23) is applicable to BSM models.

In these models BSM, we can consider a more general theory described by the following lagrangian

$$\mathcal{L}_{MostGeneralTheory} = \mathcal{L}_{SM} + \mathcal{L}_{BSM}, \tag{2.69}$$

where $\mathcal{L}_{BSM}$ represents extensions of the SM that explain phenomena not addressed by the SM, such as quantum gravity, dark matter, neutrino masses, matter-antimatter asymmetry, the hierarchy problem, among others. In the next chapters, we will study three popular BSM models in the literature, with a primary focus, as mentioned, on collider physics. The models of interest will be 331RHN, 331LHN, and Leptophilic Z' models.

3 The 3-3-1 RHN and LHN Models in the HL-LHC, HE-LHC and the FCC

In the preceding chapter, we observed that electromagnetic and weak interactions can be described by constructing a local gauge invariance theory based on the $SU(2)_L \times U(1)_Y$ group. This symmetry is subsequently broken through the SSB process, which, thanks to the Higgs Mechanism and the unitary gauge, prevents the production of Goldstone bosons. As a consequence of this mechanism, the vector bosons $W^{\pm}$ and Z acquire mass, and mass terms for the charged fermions emerge in the lagrangian due to their interaction with the Higgs field Φ. Additionally, a new particle, known as the Higgs boson, becomes part of the particle content. Finally, because the theory now exhibits invariance under the residual $U(1)_Q$ group, we have a massless gauge boson identified as the photon, ensuring the conservation of electric charge.

Today, it is widely accepted that the SM is not the ultimate theory regarding the interactions between elementary particles. Despite its success in passing all experimental tests, there are still fundamental questions that remain unresolved. One of the main pieces of evidence for physics BSM is related to the mass of neutrinos. As we observed in the previous chapter, within the SM, neutrinos do not possess mass since no mass terms for neutrinos, like the one shown in Eq. (2.44), appear due to the absence of right-handed neutrinos (see Eq. (2.20)). However, our current knowledge indicates that neutrinos undergo oscillations, implying that they indeed have non-zero masses—a phenomenon that contradicts the SM. Moreover, there are other open BSM problems, such as dark matter, matter-antimatter asymmetry, and grand unification theories, among others, that the SM does not address. These issues suggest that the SM requires extensions to provide a more complete picture of fundamental particles. Consequently, any extension of the SM that can accommodate these (or some of these) problems becomes a promising candidate for BSM physics.

In this chapter, we will present the main features of two theoretical frameworks: the 3-3-1 model with Right-Handed Neutrinos (331RHN) and the 3-3-1 model with Heavy Neutral Leptons (331LHN). Utilizing collider data from the ATLAS collaboration, we will derive mass limits for a new gauge boson, commonly known in the literature as the Z' boson, in future colliders like the HL-LHC (High-Luminosity LHC), the HE-LHC (High-Energy LHC), and the Future Circular Collider (FCC). Specifically, we will obtain lower mass bounds on the Z' gauge boson based on dilepton data from the LHC with a center-of-mass

energy of $\sqrt{s} = 13$ TeV. Additionally, we will forecast the sensitivity of the HL-LHC with an integrated luminosity of $L_{int} = 3000\ fb^{-1}$, the HE-LHC with a center-of-mass energy of $\sqrt{s} = 27$ TeV, and the Future Circular Collider with a center-of-mass energy of $\sqrt{s} = 100$ TeV.

3.1 The Models

Several BSM theories have been proposed to address fundamental open problems in particle physics, such as neutrino masses [15–29], dark matter (DM) [30–40, 40–55], meson anomalies [56–63], flavor violation [64, 65], among others [66–71]. One notable feature of these theories is the existence of heavy neutral resonances that decay into lepton pairs [72]. As part of their predictions, many of these models propose the existence of new spin-1 neutral gauge bosons, which can potentially be produced and detected at both present and future colliders.

For instance, at the LHC, events with missing energy could indicate the presence of new BSM particles, such as DM particles. However, the LHC can also indirectly contribute to DM research by observing the decays of new gauge bosons that mediate interactions between SM and DM particles. Among the various available channels, the dilepton channel stands out due to its relatively clean detector signal compared to the di-jet channel, offering a more favorable signal-to-background ratio for studying these interactions.

Examining collider physics offers a promising avenue to establish mass constraints on new vector bosons and explore the potential of searching for new physics models at the LHC. One notable approach involves investigating dilepton signals and their invariant masses. For instance, the observation of a dilepton signal with an invariant mass of 4 TeV would lead us to conclude that such a signal is inconsistent with a model based on the $SU(3)_C \times SU(3)_L \times U(1)_X$ gauge symmetry [17, 19–21, 33, 44, 46].

Studying BSM models based on the $SU(3)_C \times SU(3)_L \times U(1)_X$ group is important as it offers potential solutions to various open problems in particle physics. These encompass a wide range of BSM topics. Therefore, before presenting the collider analysis conducted in the $pp \to Z' \to ll$ production channel for the new Z' boson, we will discuss the main characteristics of the 331LHN and 331RHN models that are relevant to our analysis.

3.1.1 The Fermion Content

As mentioned before, the 3-3-1 models considered in this chapter extend the electroweak symmetry group of the SM, namely, $SU(2)_L \times U(1)_Y \rightarrow SU(3)_L \times U(1)_X$. This extension of the symmetry group brings about several interesting consequences from the perspective of collider phenomenology. With the extension of the SM symmetry group, new particles emerge alongside the existing SM particles. Consequently, new interactions between the SM and BSM particles arise.

To initiate the discussion of the main features of the 331LHN [33,73] and 331RHN [74,75] models relevant for constraining the mass of a new Z' boson, we begin by defining the new Gell-Mann-Nishijima relation for the electric charge operator Q. As shown previously in Eq. (2.19), we construct the charge operator Q based on the diagonal generators of the group under consideration. In the context of the 331LHN and 331RHN models, the electric charge operator is derived from the diagonal generators of the $SU(3)_L \times U(1)_X$ group. Consequently, in the 3-3-1 models, Q takes the following form

$$Q = \frac{1}{2}\left(\lambda_3 + \beta\lambda_8\right) + X\widehat{I}, \tag{3.1}$$

Here, $\lambda_{3,8}$ and $X\widehat{I}$ represent the diagonal generators of the groups $SU(3)_L$ and $U(1)_X$, respectively[1]. The parameter X denotes the charge of the $U(1)_X$ group. The parameter β defines the type of the 3-3-1 model. For the 331RHN and 331LHN models, β takes the value $\beta = -1/\sqrt{3}$[2].

For an anomaly-free theory in the 331RHN and 331LHN models, a specific arrangement of representations is required for the lepton and quark sectors: the fermions are classified into triplet and singlet representations, each with specific assignments under the $SU(3)_C \times SU(3)_L \times U(1)_X$ gauge symmetry, as follows

---

[1] The matrices λ_i correspond to the Gell-Mann matrices, serving as generators of the $SU(3)$ group.
[2] Other values of the parameter β in Eq. (3.1) correspond to alternative 3-3-1 models [ref]

$$F_{aL} = \begin{pmatrix} \nu_a \\ l_a \\ f'_a \end{pmatrix}_L \sim (\underline{1}, \underline{3}, -1/3), \quad l_{aR} \sim (\underline{1}, \underline{1}, -1), \tag{3.2}$$

$$Q_{iL} = \begin{pmatrix} d_i \\ -u_i \\ d'_i \end{pmatrix}_L \sim (\underline{3}, \underline{3}^*, 0), \quad u_{iR} \sim (\underline{3}, \underline{1}, 2/3),$$
$$d_{iR} \sim (\underline{3}, \underline{1}, -1/3), \quad d'_{iR} \sim (\underline{3}, \underline{1}, -1/3), \tag{3.3}$$

$$Q_{3L} = \begin{pmatrix} u_3 \\ d_3 \\ T \end{pmatrix}_L \sim (\underline{3}, \underline{3}, 1/3), \quad u_{3R} \sim (\underline{3}, \underline{1}, 2/3),$$
$$d_{3R} \sim (\underline{3}, \underline{1}, -1/3), \quad T_R \sim (\underline{3}, \underline{1}, 2/3), \tag{3.4}$$

where $a = 1, 2, 3$ and $i = 1, 2$ indicate the generation indices. The notation $\sim \left(\underline{g_1}, \underline{g_2}, g_3 \right)$ follows the same interpretation as discussed in the previous chapter, with the difference that $\underline{g_2}^*$ indicates that the field in question transforms as an anti-triplet under transformations of the $SU(3)_L$ group. For example, $Q_{iL} \sim (\underline{3}, \underline{3}^*, 0)$ transforms as a triplet under $SU(3)_C$ and an anti-triplet under $SU(3)_L$ with $X = 0$.

One of the main characteristics of the new BSM scenario under analysis is the new f'_a field, which corresponds to the third component of the lepton triplet F_{aL} given by Eq. (3.2). In the case of the 331RHN model, we have $f'_{aL} = \left(\nu_a^C \right)_L = (\nu_{aR})^C$, where C represents the charge conjugation operator. On the other hand, in the 331LHN model, $f'_{aL} = N_{aL}$. Additionally, a right-handed neutral fermion N_{aR} is introduced in the 331LHN model, transforming as a singlet under $SU(3)_L$ as follows

$$N_R^a \sim (\underline{1}, \underline{1}, 0) \,. \tag{3.5}$$

Finally, we can see that the model introduces three new exotic quarks, namely q' (d_i' and T).

3.1.2   The Scalar Sector and Gauge Bosons

The SSB via the Higgs mechanism and the fermion masses in the two 331RHN and 331LHN models require the following $SU(3)_L$ scalar triplets [33]

$$\chi = \begin{pmatrix} \chi^0 \\ \chi^- \\ \chi'^0 \end{pmatrix} \sim (\underline{1}, \underline{3}, -1/3) \,, \quad < \chi >_0 = \chi_0 = \begin{pmatrix} 0 \\ 0 \\ v_\chi \end{pmatrix}, \tag{3.6}$$

$$\rho = \begin{pmatrix} \rho^+ \\ \rho^0 \\ \rho'^+ \end{pmatrix} \sim (\underline{1}, \underline{3}, 2/3) \,, \quad < \rho >_0 = \rho_0 = \begin{pmatrix} 0 \\ v_\rho \\ 0 \end{pmatrix}, \tag{3.7}$$

$$\eta = \begin{pmatrix} \eta^0 \\ \eta^- \\ \eta'^0 \end{pmatrix} \sim (\underline{1}, \underline{3}, -1/3) \,, \quad < \eta >_0 = \eta_0 = \begin{pmatrix} v_\eta \\ 0 \\ 0 \end{pmatrix}. \tag{3.8}$$

Here, the VEVs of the above scalar fields, denoted as v_χ, v_ρ, and v_η, define a two-step spontaneous symmetry breaking (SSB) as follows

$$SU(3)_L \times U(1)_X \xrightarrow{\chi_0} SU(2)_L \times U(1)_Y \xrightarrow{\eta_0, \rho_0} U(1)_Q. \tag{3.9}$$

We can see from the above equation that the SSB of the 3-3-1 symmetry occurs in two steps. When the field χ acquires a VEV of $<\chi>_0 = \chi_0$, the system is no longer invariant under transformations of the $SU(3)_L \times U(1)_X$ group. However, the system is now invariant under the already known $SU(2)_L \times U(1)_Y$ symmetry of the SM (i.e., we have recovered the SM and the interactions already discussed). A second SSB occurs when the two scalars ρ and η acquire VEVs of $<\rho>_0 = \rho_0$ and $<\eta>_0 = \eta_0$, respectively. After this breaking, the system remains in the residual symmetry $U(1)_Q$, as expected. On the other hand, the more general potential, which is Lorentz invariant, renormalizable, and invariant under transformations of the group $SU(3)_L \times U(1)_X$, is the following

$$\begin{aligned}
V(\eta, \rho, \chi) =& \mu_\chi^2 \chi^2 + \mu_\eta^2 \eta^2 + \mu_\rho^2 \rho^2 + \lambda_1 \chi^4 + \lambda_2 \eta^4 + \lambda_3 \rho^4 \\
&+ \lambda_4 \left(\chi^\dagger \chi\right) \left(\eta^\dagger \eta\right) + \lambda_5 \left(\chi^\dagger \chi\right) \left(\rho^\dagger \rho\right) + \lambda_6 \left(\eta^\dagger \eta\right) \left(\rho^\dagger \rho\right) \\
&+ \lambda_7 \left(\chi^\dagger \eta\right) \left(\eta^\dagger \chi\right) + \lambda_8 \left(\chi^\dagger \rho\right) \left(\rho^\dagger \chi\right) + \lambda_9 \left(\eta^\dagger \rho\right) \left(\rho^\dagger \eta\right) \\
&- \frac{f}{\sqrt{2}} \epsilon^{ijk} \eta_i \rho_j \chi_k + h.c.,
\end{aligned} \tag{3.10}$$

where μ_χ, μ_η, μ_ρ, f and λ_i (for $i = 1, ..., 9$) represent free parameters. In our analysis, we initially made simplifying assumptions, specifically setting $f = v_\chi$, $\lambda_2 = \lambda_3$, and $\lambda_4 = \lambda_5$. However, it is important to note that our final conclusions are derived from precise numerical calculations, where we do not employ these simplifications.

The process of obtaining the masses of the physical bosons closely follows the procedure discussed in Subsection 2.2.3. Therefore, we determine the mass eigenstates of the CP-even scalars, which include S_1, S_2, and the Higgs boson h, and calculate their respective masses. We obtain

$$m_{S_1}^2 = \frac{v^2}{4} + 2\lambda_1 v_\chi^2,$$
$$m_{S_2}^2 = \frac{1}{2}\left[v_\chi^2 + 2v^2\left(2\lambda_2 - \lambda_6\right)\right], \tag{3.11}$$
$$m_h^2 = v^2\left(2\lambda_2 + \lambda_6\right).$$

In contrast, we find that only one pseudoscalar mass eigenstate, P_1, remains, with the following mass

$$m_{P_1}^2 = \frac{1}{2}\left(v_\chi^2 + \frac{v^2}{2}\right). \tag{3.12}$$

Within the spectrum of physical scalars, there also emerges a neutral complex scalar ϕ, along with two electrically charged scalars $h_1^\pm$ and $h_2^\pm$, each with the following masses

$$m_\phi^2 = \frac{1}{2}\left(\lambda_7 + \frac{1}{2}\right)\left(v^2 + v_\chi^2\right),$$
$$m_{h_1^\pm}^2 = \frac{1}{2}\left(\lambda_8 + \frac{1}{2}\right)\left(v^2 + v_\chi^2\right), \tag{3.13}$$
$$m_{h_2^\pm}^2 = \frac{v_\chi^2}{2} + \lambda_9 v^2.$$

Similarly to what was shown in the previous chapter, after spontaneous SSB, gauge bosons acquire their masses from the kinetic terms of the Higgs fields. Their masses are as follows

$$m_{Z'}^2 = \frac{g^2}{3 - 4S_W^2}\left(C_W^2 v_\chi^2 + \frac{v_\rho^2 + v_\eta^2\left(1 - 2S_W^2\right)^2}{4C_W^2}\right),$$
$$m_{W'}^2 = \frac{g^2}{4}\left(v_\eta^2 + v_\chi^2\right), \quad m_{U^0}^2 = \frac{g^2}{4}\left(v_\rho^2 + v_\chi^2\right), \tag{3.14}$$

where $v = \sqrt{v_\eta^2 + v_\rho^2} \simeq 246$ GeV, g represents the $SU(2)_L$ gauge coupling, $c_W \equiv \cos\theta_W$, and $s_W \equiv \sin\theta_W$, with θ_W being the Weinberg angle. In our analysis, we employ the decoupling limit, which assumes that the energy scale associated with the SSB of the 3-3-1 symmetry is significantly higher than the electroweak energy scale, i.e., $v_\chi \gg v_\eta, v_\rho$. The photon remains massless.

The Eq. (3.14) reveals a clear relationship between the gauge boson masses and the parameter v_χ. Therefore, by establishing an upper limit on the Z' gauge boson mass, we can subsequently impose constraints on the masses of the W' and U^0 gauge bosons. It is important to note that the W', Z', and U^0 bosons have comparable masses due to their interdependence through Eq. (3.14).

One last important result that we can derive from the 331RHN and 331LHN models is the neutral current of the boson Z' with the fermions f of the SM. This current allows us to derive, as we will show later, the limits on the mass of the Z' using the high-mass dilepton resonance searches at the ATLAS detector. The current has the following form

$$\mathcal{L}^{NC}_{Z'ff} = \frac{g}{2C_W} f\gamma^\mu \left[g'^{(f)}_V + \gamma^5 g'^{(f)}_A \right] f Z'_\mu, \tag{3.15}$$

Table 3 – Interactions of the Z' with fermions f in the 331LHN and 331RHN models.

Interactions	$g'^{(f)}_V$	$g'^{(f)}_A$
$Z'\overline{u}u, Z'\overline{c}c$	$\frac{3-8S_W^2}{6\sqrt{3-4S_W^2}}$	$-\frac{1}{2\sqrt{3-4S_W^2}}$
$Z'\overline{t}t$	$\frac{3+2S_W^2}{6\sqrt{3-4S_W^2}}$	$-\frac{1-2S_W^2}{2\sqrt{3-4S_W^2}}$
$Z'\overline{d}d, Z'\overline{s}s$	$\frac{3-2S_W^2}{6\sqrt{3-4S_W^2}}$	$-\frac{3-6S_W^2}{6\sqrt{3-4S_W^2}}$
$Z'\overline{b}b$	$\frac{3-4S_W^2}{6\sqrt{3-4S_W^2}}$	$-\frac{1}{2\sqrt{3-4S_W^2}}$
$Z'\overline{l}l$	$\frac{-1+4S_W^2}{2\sqrt{3-4S_W^2}}$	$\frac{1}{2\sqrt{3-4S_W^2}}$
$Z'\overline{N}N$	$\frac{4\sqrt{3-4S_W^2}}{9}$	$-\frac{4\sqrt{3-4S_W^2}}{9}$
$Z'\overline{\nu}_l\nu_l$	$\frac{\sqrt{3-4S_W^2}}{18}$	$-\frac{\sqrt{3-4S_W^2}}{18}$
$Z'\overline{d}'_i d'_i$	$-\frac{3-5S_W^2}{3\sqrt{3-4S_W^2}}$	$\frac{1-S_W^2}{\sqrt{3-4S_W^2}}$
$Z'\overline{T}T$	$\frac{3-7S_W^2}{3\sqrt{3-4S_W^2}}$	$-\frac{1-S_W^2}{\sqrt{3-4S_W^2}}$

where $g'^{(f)}_V$ ($g'^{(f)}_A$) are the vector (axial) coupling constant of fermions $f = l, N, q'$

with Z' (see Table 3).

3.2 Collider Constraints

3.2.1 Signal Output and Some Considerations

To perform our collider simulation, we use MadGraph5 [76, 77]. Additionally, we calculate the decay width using CalcHEP [78, 79]. These two computational tools provide accurate results for the cross-sections and decay widths of the processes under consideration. We compute the $pp \to Z' \to ll$ process at $\sqrt{s} = 13$ TeV, where $l = e$, μ and compare our findings with the public results from the ATLAS Collaboration [80].

To simulate the cross-section of the Drell-Yan process, we generate Monte Carlo events using the parton distribution function (PDF) NNPDF23LO [81]. For our event selection criteria, we specifically require the presence of two oppositely charged leptons. Moreover, to enable a direct comparison with the ATLAS Collaboration data, we apply certain kinematic cuts for the selected leptons: $p_T > 30$ GeV and $|\eta| < 2.5$[3]. In contrast to previous studies that solely focused on Z' interactions with fermions, we take a comprehensive approach by fully implementing the entire model using the FeynRules package [82, 83]. This implementation allows us to generate output files for both CalcHEP and MadGraph5, enabling a more thorough and detailed exploration of the model interactions and predictions.

To calculate the branching ratio of the Z' into leptons, we use

$$Br\left(Z' \to l\bar{l}\right) = \frac{\Gamma\left(Z' \to l\bar{l}\right)}{\Gamma_{Z'}}, \tag{3.16}$$

with

---

[3] The transverse momentum p_T defined as $p_T = \sqrt{p_x^2 + p_y^2}$, are the magnitude of the momentum components that are transverse to the beam axis (is usual to set the beam axis in the z direction). The geometrical variable pseudorapidity η, defined as $\eta = ln\frac{\theta}{2}$, is a variable that relates the transverse coordinates with the z-axis.

$$\Gamma_{Z'} = \sum_X \Gamma\left(Z' \to 2X\right), \tag{3.17}$$

where X represents the SM and BSM particles in the 3-3-1 models under consideration, and $l = e, \mu$. An important aspect considered in our analysis is the calculation of the branching ratio. The total and partial decay width into dileptons were performed at leading order. For the total width, the calculation is comprehensive and encompasses all feasible decay channels, including those involving new gauge bosons, scalars, exotic quarks, and neutral heavy leptons (which, under very specific conditions, could be considered as dark matter). We ensured that all potential decay channels were taken into consideration during our analysis. As seen in Eq. (3.11)-Eq. (3.14), we have explicitly written the scalar masses to emphasize their relevance to our analysis. It is important to note that $m_{Z'} \approx 0.3 v_\chi$, and the relevant Z' interactions include $Z'\phi\phi^*$, $Z'W'h_1^-$, $Z'h_1^+h_1^-$, $Z'h_2^+h_2^-$, $Z'W^+h_2^-$, $Z'S_1P_1$, among others.

Examining Eq. (3.11) through Eq. (3.14), it becomes evident that the scalar particles possess significantly higher masses compared to the Z' gauge boson. As a result, they do not contribute to the two-body decay width of the Z' boson given by Eq. (3.17). While three-body decay widths are theoretically possible, they are expected to be suppressed due to the large mass of the scalar particles relative to the Z' gauge boson. Furthermore, considering the substantial mass difference between the scalars and the Z' gauge boson, the scalar fields remain beyond the reach of the LHC. As a result, scalar fields do not offer a potential signature for detecting a 3-3-1 symmetry at the LHC. In summary, in our analysis, the role of scalar fields in the 3-3-1 model is negligible within the LHC context.

Based on all the above discussions, we can confidently assert that scalar fields do not significantly impact our collider phenomenology. Another similar situation arises in relation to the new gauge bosons. Due to the comparable masses of the exotic gauge bosons, the decays of Z' into exotic boson pairs are kinematically forbidden. However, it is important to note that there are important exotic decays involving new neutral leptons and exotic quarks. Considering additional exotic decays (related to the new neutral leptons N_i and exotic quarks q') of the Z' gauge boson holds significance as it can notably diminish the lower mass bounds derived from dilepton data[4]. To assess the impact of each potential new decay channel, we investigate several benchmark (BM)

---

[4]   When substantial decay channels are introduced, they contribute to the total width, leading to a reduction in the branching ratio into dileptons. Consequently, this results in weaker constraints on the mass bounds.

Table 4 – Different benchmarks considered for the analysis.

Model	3-3-1 LHN		3-3-1 RHN
Mass (in TeV)	$m_{q'}$	m_N	$m_{q'}$
BM1	10	10	10
BM2	1	10	1
BM3	1.5	10	1.5
BM4	2	10	2
BM5	2	2	not applicable
BM6	2	2.5	not applicable
BM7	2	4	not applicable
BM8	1	1	not applicable
BM9	0.5	10	not applicable
BM10	10	0.5	not applicable

models, varying the masses of the new neutral leptons and exotic quarks, to quantify their importance in the derivation of lower mass bounds, as shown in Table 4. By systematically exploring these scenarios, we gain valuable insights into the relative importance of each decay channel and its influence on the overall constraints and predictions of the model.

3.3   Results and Discussions

A. Branching Ratios.

In both 3-3-1 models, the partial widths of the Z' gauge boson into charged leptons l, $\Gamma(Z' \rightarrow ll)$, remain identical due to their same couplings (as depicted in Eq. (3.15) and Table 3). However, the branching ratio into charged leptons, $Br(Z' \rightarrow ll)$, can exhibit significant modifications between the two models. This discrepancy arises due to the presence of neutral leptons N_i (exclusive to the 331LHN model) and exotic quarks q' (found in both the 331LHN and 331RHN models). The inclusion of these particles has a significant impact on the total width, leading to potential modifications in the branching ratios involving charged leptons. Therefore, only when decays into N_i pairs are inaccessible, both models are indistinguishable as far as $Z' \rightarrow ll$ searches are concerned.
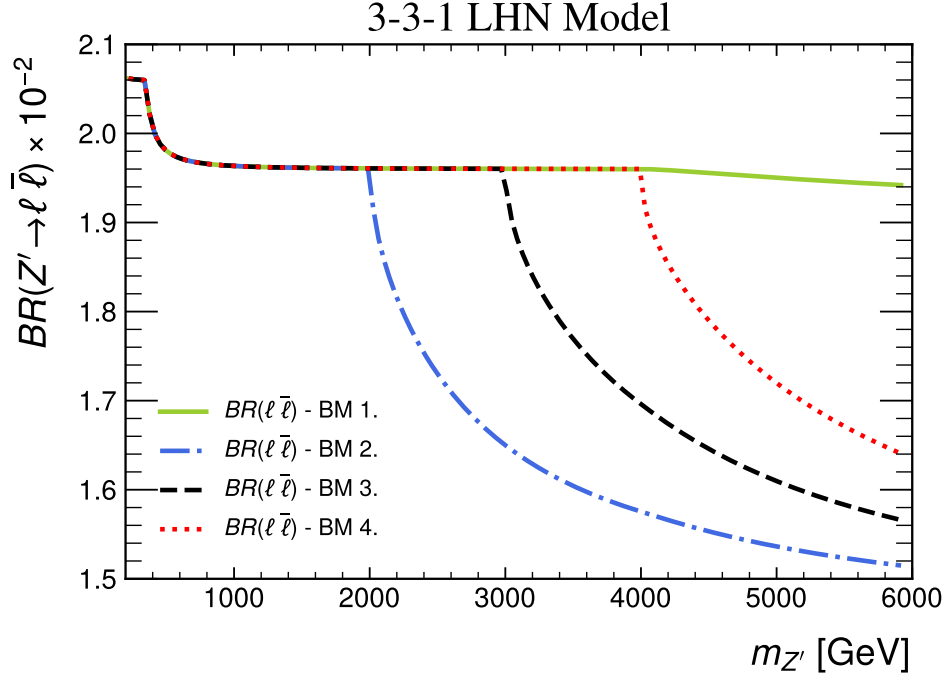
Figure 2 – Branching ratio for the Z' decay into dilepton channel as a function to $m_{Z'}$ for the benchmark sets BM1, BM2, BM3, and BM4 of the 3-3-1 LHN model.
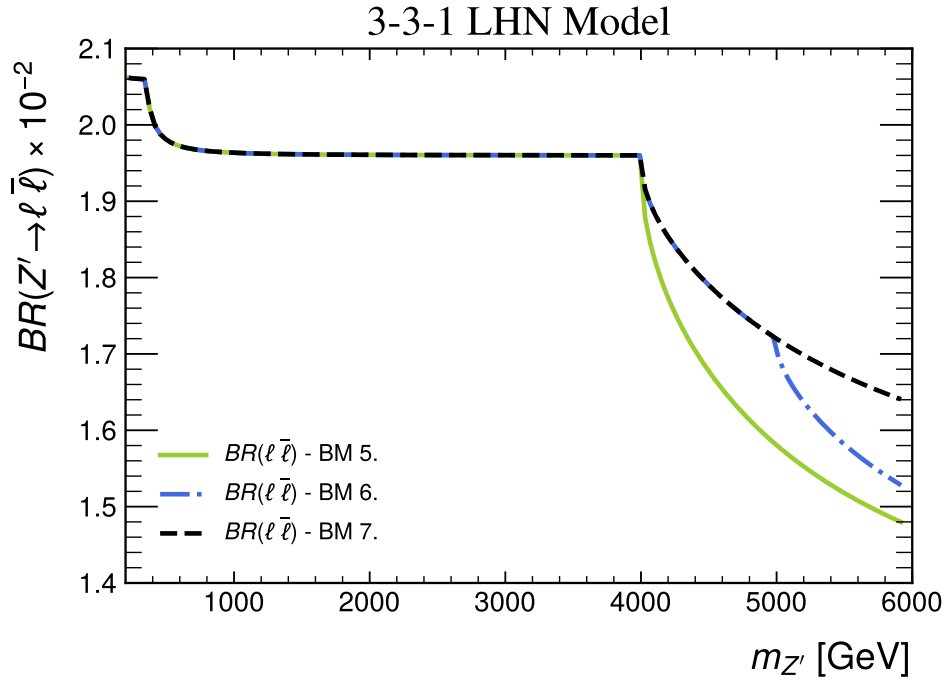
Figure 3 – Branching ratio for the Z' decay into dilepton channel as a function of $m_{Z'}$ for the benchmark sets BM 5, 6 and 7 of the the 3-3-1 LHN model.

In Figure 2 to Figure 5, we present the results of the branching ratio $Br\left(Z' \to ll\right)$ as a function of $m_{Z'}$ for various BM in both the 3-3-1 RHN and LHN models. We can
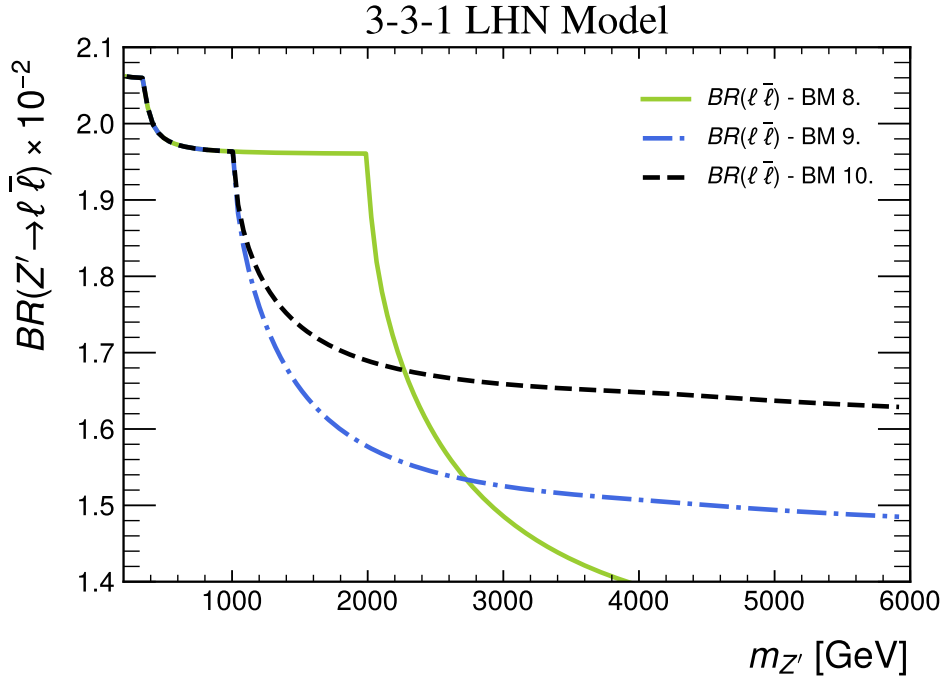
3-3-1 LHN Model

Figure 4 – Branching ratio for the Z' decay into dilepton channel as a function to $m_{Z'}$ for the benchmark sets BM 8, 9, and 10 the 3-3-1 LHN model.
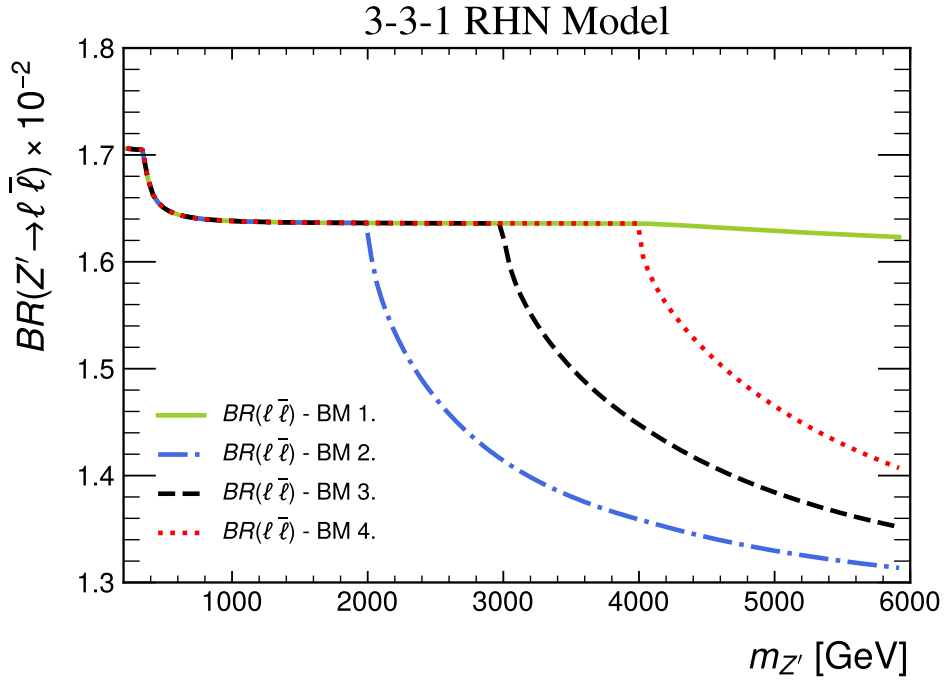
3-3-1 RHN Model

Figure 5 – Branching ratio for the Z' decay into dilepton channel as a function to $m_{Z'}$ for the 3-3-1 RHN model.

see that in both models, the branching ratio is observed to be less than 2.% and 1.7.%, respectively. In Figure 2, when considering the 331LHN model, the BM 2-3-4 demonstrate a distinct drop in the branching ratio at approximately $m_{Z'} = 2000$ GeV, 3000 GeV, and 4000 GeV, respectively. This behavior is a consequence of the decay of the Z' gauge boson

into exotic quarks q'. In contrast, since the masses of the new exotic quarks are fixed at 10 TeV, the BM1 configuration does not exhibit similar behavior. This fixed higher mass of the exotic quarks in the BM1 scenario prevents the occurrence of the observed drop in the branching ratio, distinguishing it from the BM 2-3-4.

Similarly, within the 331LHN model, we observed a significant decrease in the branching ratio into charged leptons for the BM 5, 6, and 7 when $m_{Z'} = 4000$ GeV (Figure 3). This decrease is attributed to the presence of exotic quarks at $m_{q'} = 2000$ GeV. This effect is notably evident in BM6, where the decays into heavy neutral fermions N_i is kinematically allowed. When $m_{Z'}$ approaches around 5 TeV, with a fixed mass of $m_{N_i} = 2.5$ TeV, BM6 exhibits a significant reduction in the branching ratio. A similar situation is shown in Figure 4.

In the 331RHN model, we find that the behavior of the branching ratio is comparable to that of the 331LHN model. By subjecting the exotic quark masses to the same variations, we observe a similar decrease in the branching ratio, as depicted in Figure 5. However, a notable difference arises in the size of the branching ratio into charged leptons. In the 331RHN model, this branching ratio is relatively smaller compared to the 331LHN model. This discrepancy arises because the Z' gauge boson can always decay into right-handed neutrinos, which are assumed to have masses in the keV range [84]. This distinctive feature contributes to the reduced branching ratio into charged leptons in the 331RHN model.

B. Signal Production.

As mentioned previously, we utilized `MadGraph5` and `CalcHEP` to simulate the production of a Z' gauge boson at the LHC with its subsequent decay into dileptons ($l = e, \mu$). To perform a direct comparison with the ATLAS Collaboration data presented in Fig. 3(a) of reference [80], we plot the cross-section $\sigma_{fid}(pp \rightarrow Z') \times Br(Z' \rightarrow ll)$ as a function of $m_{Z'}$ for both the 331RHN and 331LHN models[5]. The results of this comparison are depicted in Figure 6. For the Z' mass, we take different values in the interval of 200 GeV $< m_{Z'} < 6000$ GeV with steps of 40 GeV. To derive the lower mass bounds on the Z' gauge boson, we identify their values using the intersection between the red solid curve and the following lines in Figure 6(a), Figure 6(b), Figure 6(c), Figure 6(d): The solid red and dashed black lines symbolize $\sigma_{fid.} \times BR(ll)$ upper limits observed and expected at 95% C.L. as a function of Z' mass for the 10% width signals for the dilepton channel $Z' \rightarrow ll$ in the ATLAS experiment at a center of mass energy 13 TeV (ATLAS Collaboration).

---

[5] The fiducial cross-section σ_{fid} is a measure of the rate at which a certain type of collision or interaction occurs within a specific range of experimental conditions.

(a) $\sigma_{fid.} \times BR\,(ll)$ vs $m_{Z'}$ for BM sets 1, 2 and 3 in the 3-3-1 RHN model.

(b) $\sigma_{fid.} \times BR\,(ll)$ vs $m_{Z'}$ for BM sets 1, 2 and 3 in the 3-3-1 LHN model.

(c) $\sigma_{fid.} \times BR\,(ll)$ vs $m_{Z'}$ for BM sets 5, 6 and 7 in the 3-3-1 LHN model.

(d) $\sigma_{fid.} \times BR\,(ll)$ vs $m_{Z'}$ for BM sets 8, 9 and 10 in the 3-3-1 LHN model.
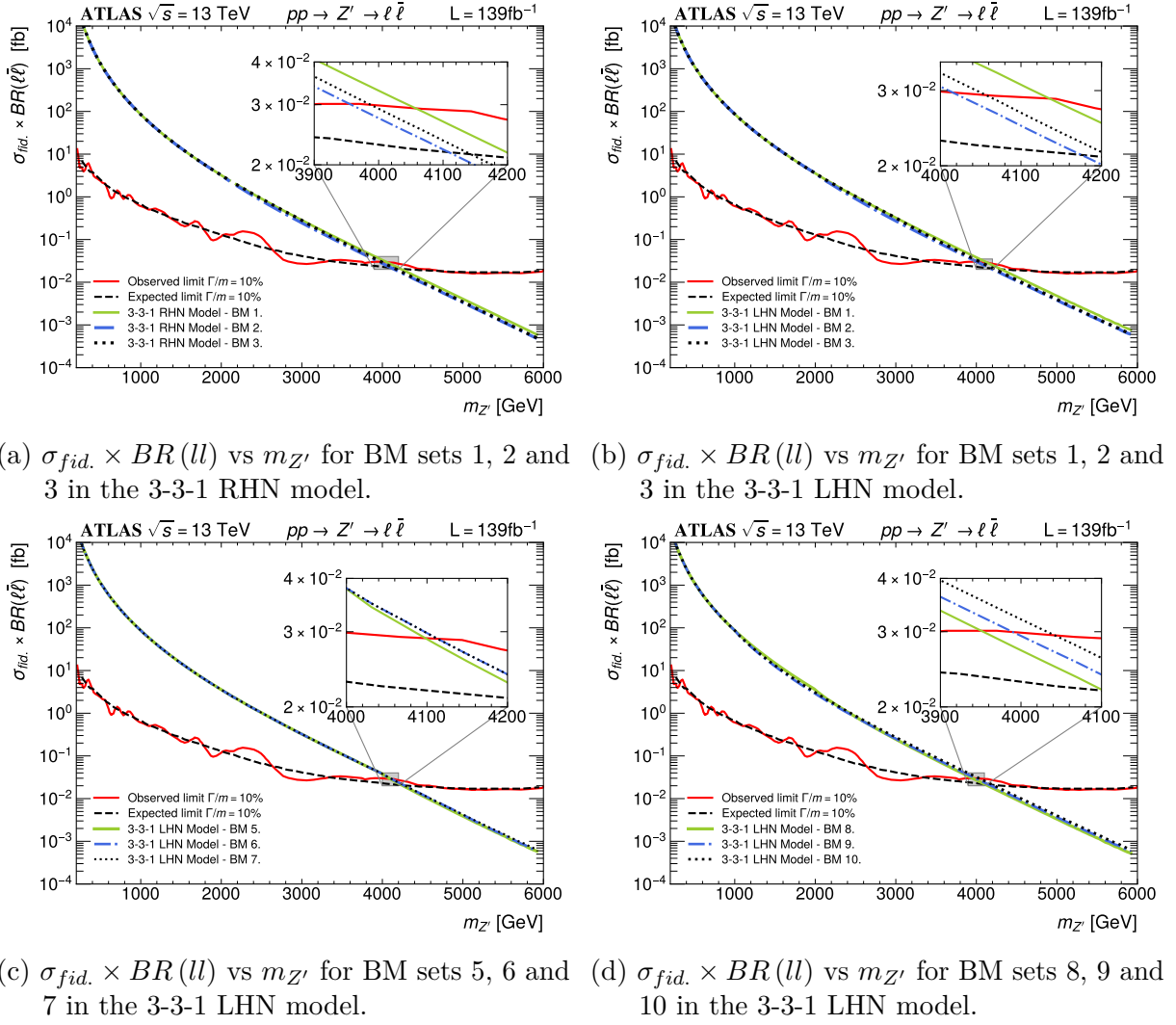
Figure 6 – $\sigma_{fid.} \times BR\,(ll)$ vs $m_{Z'}$ for differents benchmark configurations in the 3-3-1 LHN and RHN models.

The solid yellowgreen, dash-dot blue, and black dotted lines represent the theoretical production $\sigma_{fid}\,(pp \to Z') \times BR\,(Z' \to ll)$ generated using `MadGraph5` and `CalcHEP` for several benchmark sets for the 3-3-1 RHN and LHN models. We assume different masses for the new exotic quarks and heavy neutral lepton (see Table 4). The specific results obtained from this analysis are shown in Table III.

C. HE-LHC, HL-LHC and FCC-hh colliders.

Once we have determined the lower bounds for $m_{Z'}$ using data from the 13 TeV LHC with an integrated luminosity of 139 fb^{-1} (as presented in Table III), we utilize these results as input for the `Collider Reach` β. Subsequently, we derive the expected limits for the HL-LHC, HE-LHC [85], and Future Circular Collider with hadron-hadron collisions (FCC-hh) setups [86].

Table 5 – Lower mass bounds on Z' boson for different benchmark models.

Model	BM	$m_{Z'}$ (GeV)
331RHN	BM 1	4052
	BM 2	3960
	BM 3	3989
	BM 4	4040
331LHN	BM 1	4132
	BM 2	4013
	BM 3	4060
	BM 4, 6 and 7	4118
	BM 5	4094
	BM 8	3950

We set the following collider configurations:

(I) HE-HL: For the center-of-mass energy $\sqrt{s}$=13, 14 and 27 TeV, and integral luminosity L_{int}=139 fb^{-1}, 300 fb^{-1}, 500 fb^{-1} and 3000 fb^{-1}.

(II) FCC-hh: For the center-of-mass energy $\sqrt{s}$=100 TeV and integral luminosity L_{int}=139 fb^{-1}, 300 fb^{-1}, 500 fb^{-1} and 3000 fb^{-1}.

Tables 6 and 7 presents the mass reach for the HE-HL LHC and FCC-hh colliders. At the HL-LHC, we observe an increase in the expected lower mass bounds by 1.2–1.5 TeV when compared to the 139 fb^{-1} data (Table 5). Notably, in the case where the integrated luminosity reaches 3000 fb^{-1} and the center-of-mass energy of $\sqrt{s} = 14$ TeV, the projected sensitivity improves by nearly 2 TeV for certain benchmarks.

The lower mass bounds witness substantial enhancements at the 27 TeV HE-LHC and the 100 TeV FCC-hh collider, both with an integrated luminosity of $L_{int} = 3000$ fb^{-1}. Specifically, these bounds improve by a factor of approximately 2.5 and 7, respectively, in comparison to the values obtained at the LHC with a center-of-mass energy of $\sqrt{s} = 13$ TeV and an integrated luminosity of 139 fb^{-1} (as detailed in Table 5). Additionally, it is worth noting that BM1 and 3 in the 331RHN model correspond to BM10 and 9 in the 331LHN model, respectively. Similarly, BM6 and 7 exhibit a similar bound to BM4 in

Table 6 – Different $m_{Z'}$ reaches for all BM sets considered in the 331RHN model at HL-HE LHC and FCC-hh.

BM sets	L_{int} (fb^{-1})	$m_{Z'}$-13 TeV	$m_{Z'}$-14 TeV	$m_{Z'}$-27 TeV	$m_{Z'}$-100 TeV
BM 1[6]	139	4.052	4.288	6.987	17.180
	300	4.390	4.651	7.675	19.447
	500	4.613	4.892	8.136	21.006
	1000	4.916	5.217	8.763	23.175
	3000	5.388	5.727	9.755	26.711
BM 2	139	3.960	4.189	6.801	16.548
	300	4.298	4.552	7.487	18.821
	500	4.521	4.793	7.947	20.363
	1000	4.825	5.119	8.574	22.514
	3000	5.298	4.699	9.566	26.030
BM 3[7]	139	3.989	4.220	6.860	16.769
	300	4.327	4.583	7.547	19.016
	500	4.550	4.824	8.006	20.564
	1000	4.853	5.149	8.633	22.721
	3000	5.326	5.661	9.626	26.244
BM 4	139	4.040	4.275	6.963	17.101
	300	4.378	4.638	7.651	19.364
	500	4.601	4.879	8.111	20.921
	1000	4.904	5.204	8.739	23.089
	3000	5.377	5.715	9.731	26.652

the 331LHN model, and these observations can be readily explained by considering the presence or absence of exotic Z' decays, as discussed earlier.

So far we have seen that one of the ways to study physics BSM is to extend the symmetry group of the SM. Extending the symmetry group allows the emergence of new particles in addition to the SM particles and as a consequence new interactions appear that could explain phenomena that the SM does not incorporate and that we can study in the context of particle collider physics. As we saw in this chapter, the 3-3-1 LHN and RHN models are one of these extensions, and among the various phenomenological consequences, they predict the existence of new fermions, new scalars and gauge bosons. As we saw in

Table 7 – Different $m_{Z'}$ reaches for all BM sets considered in the 331LHN model at HL-HE LHC and FCC-hh.

BM sets	L_{int} (fb^{-1})	$m_{Z'}$-13 TeV	$m_{Z'}$-14 TeV	$m_{Z'}$-27 TeV	$m_{Z'}$-100 TeV
BM 1	139	4.132	4.374	7.149	17.709
	300	4.470	4.737	7.839	19.990
	500	4.693	4.978	8.301	21.571
	1000	4.995	5.303	8.928	23.755
	3000	5.467	5.812	9.920	27.306
BM 2	139	4.013	4.246	6.908	16.924
	300	4.351	4.609	7.596	19.197
	500	4.574	4.850	8.056	20.731
	1000	4.877	5.175	8.683	22.894
	3000	5.350	5.686	9.675	26.421
BM 3	139	4.060	4.297	7.003	17.233
	300	4.398	4.660	7.692	19.502
	500	4.621	4.901	8.153	21.062
	1000	4.924	5.225	8.780	23.233
	3000	5.396	5.736	9.772	26.770
BM 4,6,7	139	4.118	4.359	7.121	17.616
	300	4.456	4.722	7.811	19.902
	500	4.679	4.963	8.272	21.472
	1000	4.981	5.288	8.900	23.654
	3000	5.453	5.797	9.891	27.202
BM 5	139	4.094	4.333	7.072	17.457
	300	4.432	4.696	7.761	19.736
	500	4.655	4.937	8.223	21.302
	1000	4.958	5.262	8.850	23.479
	3000	5.430	5.772	9.842	27.023
BM 8	139	3.950	4.178	6.781	16.520
	300	4.288	4.541	7.467	18.753
	500	4.511	4.782	7.926	20.294
	1000	4.815	5.108	8.553	22.443
	3000	5.289	5.620	9.546	25.956

this chapter, although a new Z' boson from these models has not been directly detected by particle colliders like the LHC, we were able to constrain its mass using data from the LHC and extrapolate for its upgrades known as HL-LHC, HE-LHC, as well as the projected Future Circular Collider in hadron-hadron collisions (FCC-hh).

However, as we will see in the next chapter, there are other, simpler ways to propose BSM physics and study its impacts on other future colliders, such as electron-positron colliders.

4 The 331LHN, 331RHN and Z' Leptophilic in the Compact Linear Collider

In the previous chapter, we delved into the possibility of utilizing hadron collider data to constrain the mass of a new Z' boson originating from the 331LHN and 331RHN models. This chapter introduces a slightly distinct focus compared to the preceding one. Here, we will delve deeper into the potential discovery of a new Z' boson emerging from the aforementioned models, along with the Z' of a simplified model known in the literature as the "leptophilic Z'". Our investigation will unfold within the framework of the Compact Linear Collider (CLIC), a particle collider designed for e^+e^- collisions that will operate at a center-of-mass energy of 3 TeV.

Motivated by the importance of a new Z' boson emerging from extensions of the SM, like the 3-3-1 models or other simplified models, our objective is to investigate the DY production channel $pp \to Z' \to ll$ analyzing the impact of the signal vs background at CLIC. This investigation involves an analysis of kinematic cuts on the transverse momentum p_T, pseudorapidity η, and invariant mass M for the two leptons in the final state.

The CLIC collaboration is projected to be a global cooperative effort situated within the CERN facilities [87]. Its primary aim is to construct a linear e^+e^- collider operating at the TeV scale while maintaining high luminosity. In order to fully leverage its potential for BSM physics, CLIC is strategically designed to be implemented in progressive stages. The projected operational energies for each of CLIC's three stages are 380 GeV, 1.5 TeV, and 3 TeV, respectively. The anticipated spatial range for its footprint spans between 11 km and 50 km.

Recent times have witnessed significant advancements in the technical refinement and rigorous testing of CLIC accelerator systems. These breakthroughs have not only led to cost reductions in construction but have also enhanced the collider's physics capabilities. Set to commence operations around 2035, the inaugural beam injection heralds the beginning of an expansive physics program projected to unfold over 25 to 30 years. Drawing from the experience gained from the Large Electron-Positron collider (LEP) [88,89], CLIC emerges as a promising avenue for exploring physics BSM. With its high luminosity and increased center-of-mass energy, CLIC stands ready to facilitate direct investigations and

enable precise measurements spanning a wide range of both SM and BSM processes. This potential is particularly relevant in the examination of the Higgs boson, expanded scalar sectors, new gauge bosons, and other phenomena.

As demonstrated in the preceding chapter, various theories that extend the SM, such as the 3-3-1 models, are rooted in the existence of neutral gauge bosons engaged in interactions with fermions. These theories have the potential to illuminate unresolved mysteries that defy explanation within the framework of the SM. These neutral bosons are often linked to a new abelian gauge symmetry, one that undergoes spontaneous breaking, thus giving rise to a Z' boson with a mass approximating the scale of new physics. Alternatively, a Z' boson can emerge from non-abelian gauge symmetries. These Z' bosons can potentially manifest themselves in hadron and lepton colliders, generating dilepton resonances, for example. From an experimental point of view, a Z' boson essentially represents a resonance, possessing a higher mass compared to the Z boson. However, from the perspective of theoreticians, a Z' field embodies a new force carrier, showing the way for the exploration of BSM physics.

Motivated by the importance of Z' bosons in theoretical constructions, our goal is to evaluate CLIC's potential for discovering both a leptophilic Z' and a Z' originating from extended gauge sectors characterized by $SU(3)_C \times SU(3)_L \times U(1)_X$ symmetry. A leptophilic Z' arises within straightforward gauged lepton number theories [90–101], as well as in more intricate configurations [102–108]. As illustrated in the preceding chapter, the $SU(3)_C \times SU(3)_L \times U(1)_X$ symmetry has been extensively explored in existing literature due to its ability to address challenges such as neutrino masses, dark matter, flavor puzzles, and the number of fermion generations.

In the context of linear colliders, past studies have investigated leptophilic Z' bosons [91, 107–110, 110–113]. However, none of these efforts have focused on a sequential leptophilic Z' boson. This boson, which couples to SM leptons similarly to the Z boson but lacks interactions with quarks, remains unexplored. Sequential Z' bosons are often the subject of collider searches at the LHC. When couplings with quark are removed, a sequential leptophilic Z' naturally emerges as a consequence, potentially serving as a reference model at CLIC. Notably, in scenarios devoid of quark interactions, CLIC becomes a particularly promising avenue for exploration, despite the LHC surpassing it in reach due to its quark couplings. Furthermore, beyond its initial role in discovery, CLIC has the potential to evolve into a precision instrument after identifying a Z' boson, whether at the LHC or the HL-LHC.

Without CLIC data at present, we cannot conduct studies similar to those that were done in the previous chapter. Therefore, in this chapter, our analysis is limited to evaluating CLIC's sensitivity reach. To do this, we are going to investigate the optimal kinematic cuts on variables such as transverse momentum p_T, pseudorapidity η and electron-positron invariant mass $M(e^+e^-)$. This exploration aims to maximize signal efficiency and achieve a 5σ signal significance for a given luminosity. Before we begin our analysis, we are going to quickly show the main features of CLIC.

4.1 The Compact Linear Collider

The Compact Linear Collider, a project currently being developed by the CLIC accelerator collaboration at CERN, is designed as a high-luminosity e^+e^- linear collider with the potential to achieve multi-TeV energies. A distinctive innovation within CLIC is the adoption of the two-beam acceleration technique, employing normal conducting accelerating structures operating in the range of 70-100 MeV/m.

The Conceptual Design Report (CDR) for CLIC was made public in 2012 [114]. Its central aim was to establish the feasibility of the CLIC accelerator for reach energies up to 3 TeV. Equally important was the confirmation that the presence of particles stemming from beam-induced backgrounds and the characteristics of the luminosity spectrum would not hinder the accuracy of high-precision physics measurements [87, 114, 115]. Just as LEP and SLAC were important to test various SM predictions [88, 89], CLIC envisions a span of 27 years [116], divided into three distinct yet complementary stages, dedicated to gathering more precise electroweak measurements and identifying signals of new physics (NP).

Employing an innovative acceleration mechanism, CLIC aspires to gradually attain energies up to $\sqrt{s} = 3$ TeV along a staged progression, along with an integrated luminosity of 5 ab^{-1}. In its initial operational phase, CLIC is anticipated to work at an energy of $\sqrt{s} = 380$ GeV and a luminosity of 1 ab^{-1}. In the subsequent second and third stages, operation is projected at $\sqrt{s} = 1.5$ TeV with $\mathcal{L} = 2.5ab^{-1}$, and $\sqrt{s} = 3$ TeV with $\mathcal{L} = 5ab^{-1}$, respectively [117–120]. At each of these operational stages, the CLIC program strives to refine electroweak precision measurements of SM parameters and potentially identify both direct and indirect indications of NP [121].

These stages in which the CLIC experiment will work are tailored according to findings derived from the HL-LHC investigations. Specifically, adjustments to the center-

of-mass energy can be achieved through elongating the accelerator's length or enhancing acceleration methodologies. This distinctive approach to acceleration technology within the CLIC experiment retains the potential for conducting inquiries characterized by elevated center-of-mass energy and luminosity.

Having in mind the new physics potential of CLIC and the popular presence of Z' fields in theoretical constructions, we describe briefly the models below.

4.2   The Models

As previously mentioned, this chapter focuses on studying the capability to produce and detect a new Z' boson in the CLIC experiment. The models employed for this analysis include, firstly, the two models discussed in the preceding chapter: the 3-3-1 RHN and LHN models, so all the theory and phenomenology discussed in Section 3.1 remain valid for the purposes of this chapter. On the other hand, we also consider the Z' leptophilic model. The Z' leptophilic model presents itself as a potential and straight-forward extension to the SM[1]. Like the 3-3-1 models, its motivation lies in addressing specific experimental anomalies and phenomena that remain unexplained by the SM [16–19, 21, 22, 105, 122, 123]. The Z' boson in the leptophilic model considered in this thesis exhibit the same SM couplings to leptons. This unique attribute could lead to distinctive collider phenomenology—observable signals that can be detected in high-energy particle collider experiments. The amplified couplings between the Z' boson and leptons may result in distinct decay patterns, production rates, and other measurable phenomena. These characteristics hold the potential for exploration in forthcoming lepton colliders, such as CLIC.

Within these 3-3-1 theoretical frameworks, we consider only one benchmark scenario: we set $M_{Z'} < 2M_X$ where X are the new fermions and bosons of the theory such that the decay of the Z' into BSM particles is kinematically forbidden. In this way, the interactions that we are going to consider in the 3-3-1 models will be those corresponding to the Z' to SM fermions (see BM1 in Table 4). In the context of the leptophilic Z' model, this consideration arises naturally, given that the leptophilic Z' maintains the same fermion couplings as the SM, with the exception of its absence of quark couplings. As a result of these coupling considerations, the total decay width $\Gamma_{Z'}$ is narrower, significantly influencing the number of events of the signal that we will describe in the next subsection.

---

[1]   A leptophilic boson is a boson that only interacts with leptons. Interactions with quarks are suppressed or negligible.

To study the production of a new vector boson Z' in the CLIC experiment, we are going to use for the 3-3-1 models the neutral current lagrangian shown in the Eq. (3.15), while for In the Z' leptophilic model, we will use the part of the SM neutral current lagrangian for leptons corresponding to the Z boson that is shown in the Eq. (2.29), taking into account that we must replace the Z boson by the boson Z'.

4.3 Simulation and Analysis

Simulation of all signal and background events was carried out using `FeynRules` [83], `MadGraph5` [76], `Pythia8` [124], and `Delphes3` [125]. A total of 80000 events were generated for each Z' mass parameter, while 200000 events were generated for backgrounds. In order to simulate realistic e^+e^- collider environments at CLIC, we utilized the `clic300ll` PDF set. We do not consider the interference between the SM and the Z' since the ratio $\Gamma_{Z'}/m_{Z'}$ is small, amounting to only a few percent.
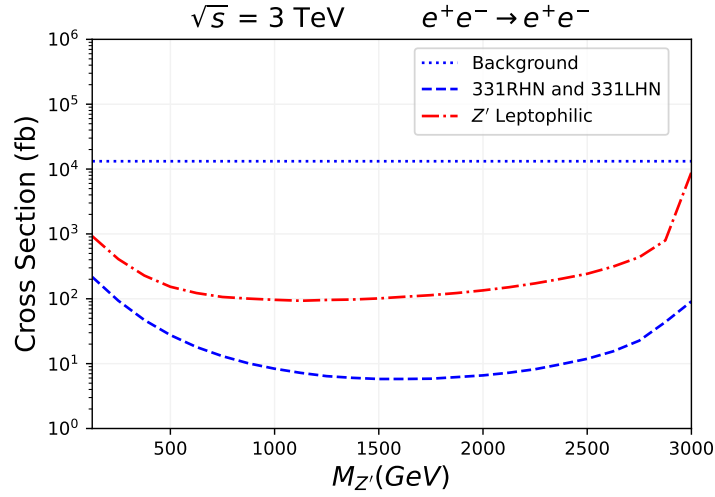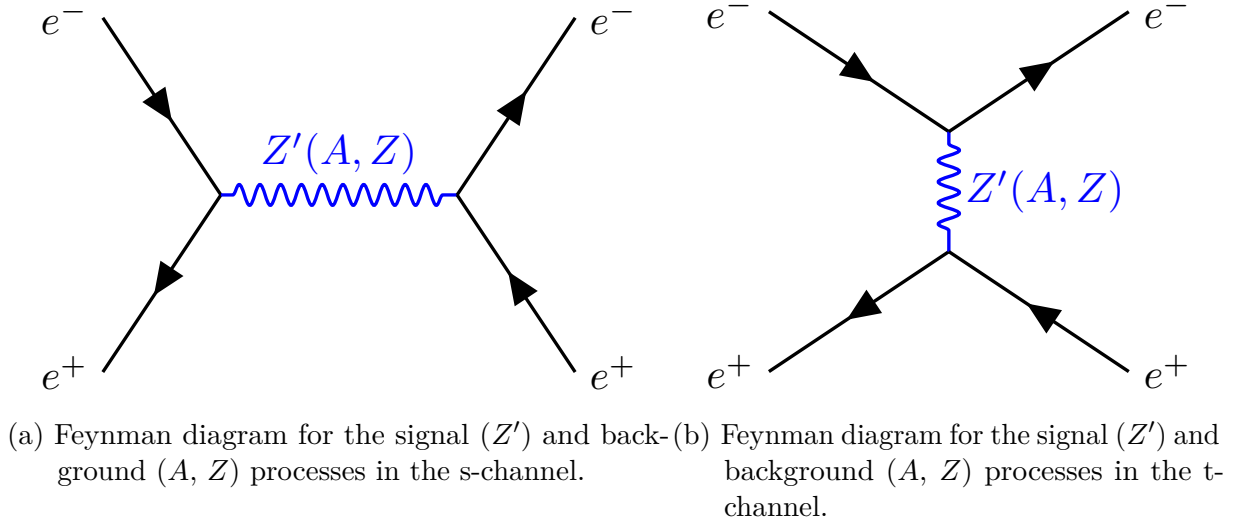
The SM background and the signal involve s and t-channel diagrams that exchange a Z boson or A (photon) for the background and a Z' boson for the signal. These diagrams are illustrated in panels (a) and (b) of Figure 7. In order to mitigate collinear divergences, we generated events that fulfill the subsequent fundamental selection criteria

$$p_T > 100 \text{ GeV}, \ \ |\eta| < 3 \ , \tag{4.1}$$

for both electron and positron in the event.

The production cross section times branching ratio into e^+e^-, after applying the basic cuts of Eq. (4.1), for 3-3-1 and leptophilic Z' bosons is presented in panel (c) of Figure 7, plotted as a function of their mass. For masses much smaller than the collider energy, the t-channel diagram dominates as the Z' is produced off its mass shell. However, heavier Z' bosons tend to be produced closer to the mass shell, leading to an increased cross section towards $M_{Z'} = 3$ TeV. On the other hand, 3-3-1 bosons exhibit a smaller cross-section due to the greater variety of decay options available to the Z', in contrast to the leptophilic case.

In both 331 and leptophilic models, the branching ratio $BR(Z' \to e^+e^-)$ is 2.4% and 11%, respectively, within the mass range considered in this study. The SM cross-section for $e^+e^- \to e^+e^-$ is 13.2 pb after applying the cuts of Eq. (4.1).

(a) Feynman diagram for the signal ($Z′$) and background (A, Z) processes in the s-channel.

(b) Feynman diagram for the signal ($Z′$) and background (A, Z) processes in the t-channel.

(c) Cross-section (in fb) for the background, 331 and $Z′$ leptophilic models.

Figure 7 – Feynman diagrams and cross-section for the signal and background processes.

The signal and background distributions for the transverse momentum p_T, rapidity η and the invariant mass $M(e^+, e^-)$, used for cuts, are displayed in Figure 8 for $Z′$ leptophilic signals. The distributions for 3-3-1 $Z′$ signals are similar and are shown in Figure 9. As we observe, the characteristics of signal and background are notably distinctive, particularly for heavy $Z′$ bosons. However, in the case of lighter $Z′$, the peaks in the e^+e^- invariant mass reveal the presence of signals, differentiating them from the smooth background spectrum.

Regarding the rapidity distributions, lighter $Z′$ particles and the SM backgrounds exhibit a comparable behavior, with the majority of events being concentrated in the high rapidity regions of the detector. On the contrary, heavy $Z′$ bosons produce central electrons and positrons. This phenomenon arises due to the interplay between the s and t-channel amplitudes. The t-channel contribution is accentuated when the final-state
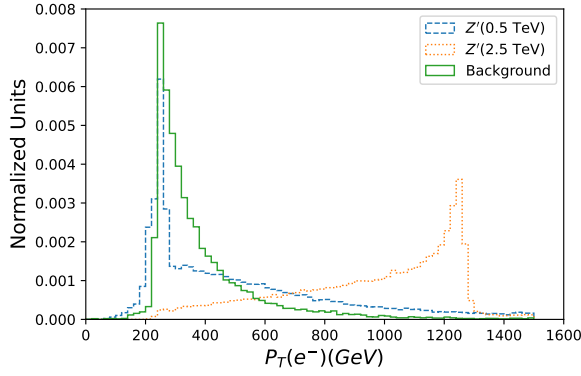
(a) Signal and background distributions for the transverse momentum of an electron in the final state corresponding to Z' masses of 0.5 and 2.5 TeV (Z' leptophilic model).
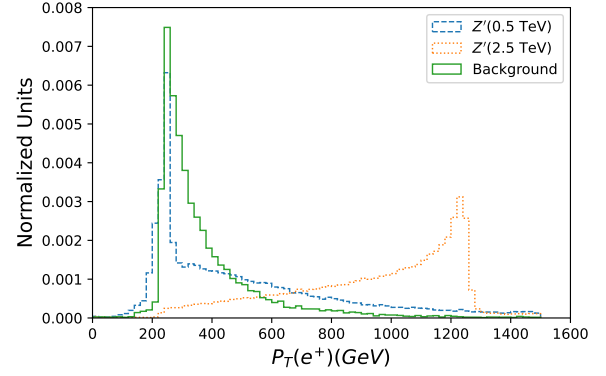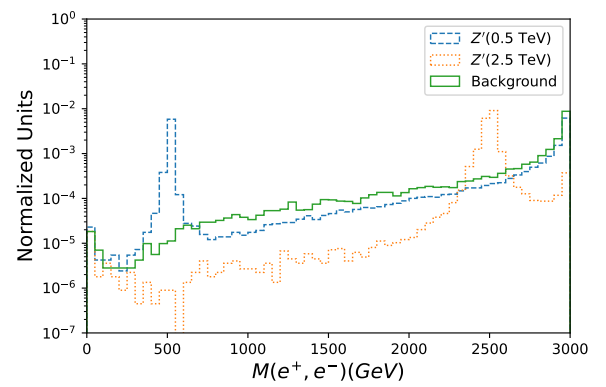
(b) Signal and background distributions for the transverse momentum of electrons in the final state corresponding to Z' masses of 0.5 and 2.5 TeV (Z' leptophilic model).
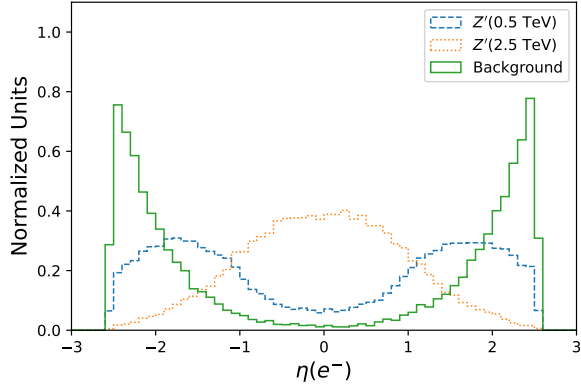
(c) Signal and background distributions for the pseudorapidity of positrons in the final state corresponding to Z' masses of 0.5 and 2.5 TeV (Z' leptophilic model).
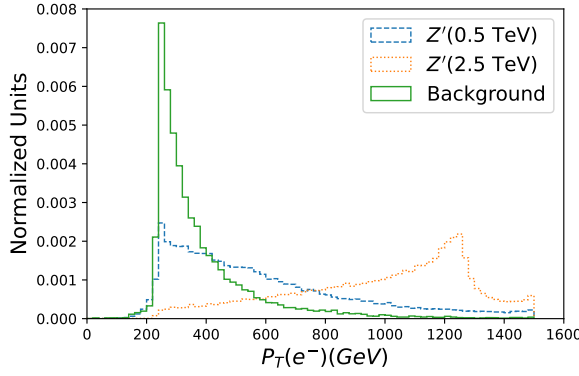
(d) Signal and background distributions for the invariant mass of an electron-positron pair in the final state corresponding to Z' masses of 0.5 and 2.5 TeV (Z' leptophilic model).

Figure 8 – Signal and background distributions for different kinematic variables corresponding to a Z' leptophilic boson with masses of 0.5 and 2.5 TeV.

lepton is collinear with the initial-state one, while the s-channel yields high-p_T outcomes.

In order to mitigate backgrounds and enhance the statistical significance of the signal, we sought optimal kinematic cuts on p_T, η and $M(e^+, e^-)$ that simultaneously maximize signal efficiency and minimize background contamination. As detailed in the subsequent section, the optimization process yielded negligible background efficiencies for Z' masses spanning from 10 GeV to 3 TeV. Subsequently, we compute the signal significance using the following formula
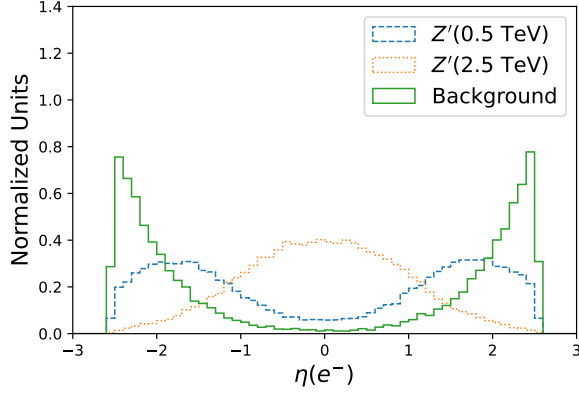
$$N_\sigma = \frac{L \times \epsilon_S \sigma_S}{\sqrt{L \times \epsilon_B \sigma_B + (\varepsilon_B^{sys} \times L \times \epsilon_B \sigma_B)^2}}. \tag{4.2}$$

(a) Signal and background distributions for the transverse momentum of an electron in the final state corresponding to Z' masses of 0.5 and 2.5 TeV (3-3-1 models).
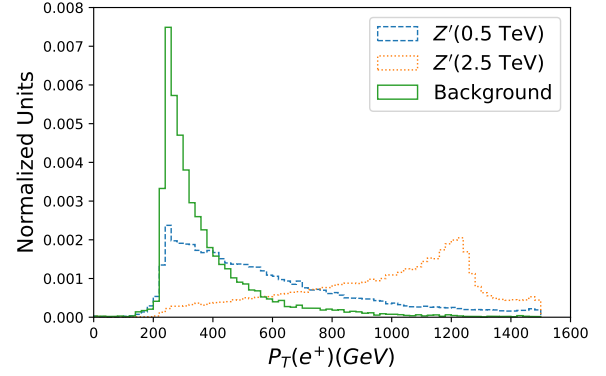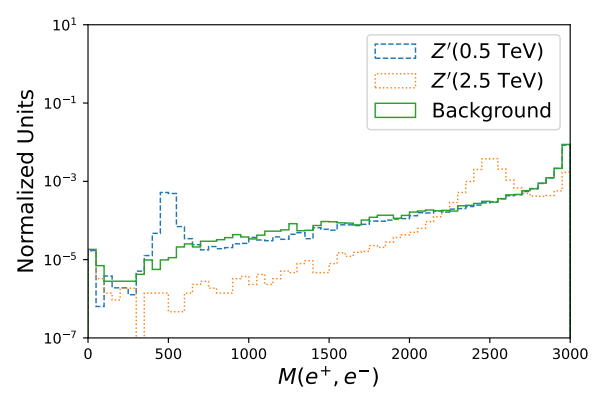
(b) Signal and background distributions for the transverse momentum of electrons in the final state corresponding to Z' masses of 0.5 and 2.5 TeV (3-3-1 models).

(c) Signal and background distributions for the pseudorapidity of positrons in the final state corresponding to Z' masses of 0.5 and 2.5 TeV (3-3-1 models).

(d) Signal and background distributions for the invariant mass of an electron-positron pair in the final state corresponding to Z' masses of 0.5 and 2.5 TeV (3-3-1 models).

Figure 9 – Signal and background distributions for different kinematic variables corresponding to a 3-3-1 Z' boson with masses of 0.5 and 2.5 TeV.

Here, σ_S (ϵ_S) and σ_B (ϵ_B) represent the cross section (selection efficiency) of the signal and backgrounds, respectively. The integrated luminosity is denoted as L, while ε_B^{sys} stands for the systematic uncertainty in the background rate. In situations where no Monte Carlo background events fulfill the selection criteria, we conservatively assume a background rate indicated by σ_B/n_{MC}, where $n_{MC} = 2 \times 10^5$, the count of simulated background events.

4.4 Results and Discussions

The Table 8 and Table 9 display the optimal cuts for certain Z' masses for the 3-3-1 and Z' leptophilic models, respectively. Here were analyzed the following kinematic variables: the electron and positron transverse momentum p_T, the electron and positron

Table 8 – The best kinematic cuts for different Z' masses in the 3-3-1 models.

$M_{Z'}$	$p_T >$	$|\eta| <$	$|M_{ee} - M_c| < \delta_M$	$\epsilon_S(\%)$
500	189	2.00	485 ± 65	11.1
1000	387	1.69	1043 ± 52	37.4
1500	444	0.92	1461 ± 88	20.1
2000	777	0.86	1970 ± 59	30.4
2500	991	0.45	2547 ± 64	15

Table 9 – The best kinematic cuts for different Z' masses in the Z' leptophilic model.

$M_{Z'}$	$p_T >$	$|\eta| <$	$|M_{ee} - M_c| < \delta_M$	$\epsilon_S(\%)$
500	207	2.23	458 ± 57	1.9
1000	420	2.1	1041 ± 51	9.3
1500	641	2.65	1554 ± 52	17
2000	531	0.85	1940 ± 80	16
2500	1032	1.96	2391 ± 84	10

pseudorapidity η and the invariant mass of a electron-positron pair M_{ee}. In the table, M_c represents the central value on the invariant mass that increment the significance and δ_M is a number around the central value. So the algorithm gives as result the cut $\delta_M < M_c < \delta_M$ on the invariant mass. All the units are in GeV. The selection of the e^+e^- mass cut involved identifying the most suitable window around the signal peak to isolate events. For that, for every Z' mass, a total of 4×10^5 random searches were conducted within the parameter space of cut thresholds encompassing the kinematic variables p_T, $|\eta|$, and the e^+e^- proximate to the signal peak. Notably, the background efficiencies remain minimal across all Z' masses, while the signal efficiency demonstrates an ascending trend from lighter to heavier Z' bosons, culminating around masses of 2.5 TeV across all model variations. From the same tables, we see that higher signal efficiencies are achieved by hardening the p_T threshold and selecting events that are more centrally produced in the detector.

The Figure 10 illustrates the luminosity required to exclude a Z' at 95% confidence level (C.L.) or to discover its signal in the 3 TeV CLIC. A 331 Z' will demand around one order of magnitude more data compared to leptophilic counterparts. Nevertheless, the less favorable scenario can be accomplished with 1 ab^{-1} of data, whereas the more promising scenarios may necessitate luminosities as modest as 100 pb^{-1}. Notably, there exists potential for enhancement by accounting for final state muons, which could potentially lead to nearly a twofold amplification of the signal cross section after implementing
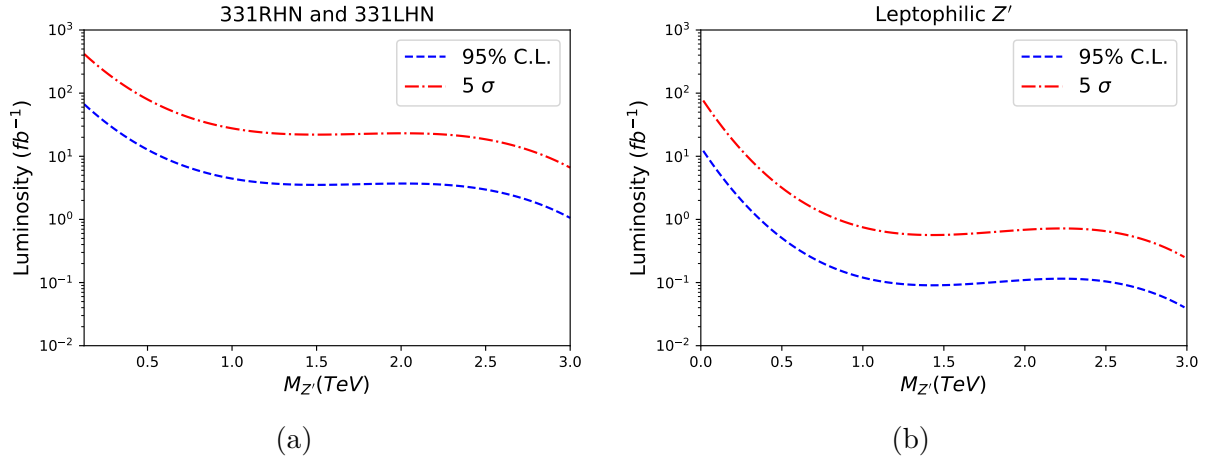
Figure 10 – Luminosity that the CLIC experiment needs to reach to detect a new Z' boson with 95% C.L. (in blue) and 5σ (in red) for the 3-3-1 models (left panel) and the Z' leptophilic model (right panel).

appropriate selection criteria, contingent upon the Z' mass.

5 Conclusions

The first part of this thesis focused on qualitatively and quantitatively explaining the concept of gauge invariance in abelian and non-abelian gauge theories. Subsequently, we detail the different sectors of the standard model lagrangian, with the aim of establishing the theoretical bases and necessary tools to describe the 331LHN and 331RHN models that will be studied in subsequent sections.

In the second part of this thesis, we established constraints from the LHC on two distinct 3-3-1 models, specifically the 3-3-1 RHN and 3-3-1 LHN frameworks. Our analysis involved evaluating the influence of the different exotic Z' decay modes in the determination of lower mass bounds using dilepton data. For that we analyze different benchmark models. Subsequently, we derived robust lower mass limits spanning from 3.9 TeV to 4.1 TeV, which exhibit notable reduction compared to prior investigations. Additionally, we projected the potential mass reach for the HL-LHC, HE-LHC, and FCC-hh experiments.

After obtaining the lower mass bounds of a Z' boson in the 3-3-1 models for different benchmarks and different future colliders, the third part of this thesis was focused on two particular models and on another experimental setup, where one of these models corresponds to one of the cases studied in the previous analysis. In the first case we analyze again the 3-3-1 models for the case where the Z' boson decays exclusively into standard model particles (BM 1 from the previous analysis). On the other hand, for the second case, we analyze a sequential Z' leptophilic model, where the couplings of the Z' with the fermions are SM like and it only couples to leptons. Analyzes were performed for the CLIC experiment. Within these theoretical frameworks and using 400K random search, we find the best kinematic cuts for the pseudorapidity η, transverse momentum p_T and invariant mass $M(e^+e^-)$ that maximizes the statistical significance of the signal for different mass values of Z'. Finally, with these data, we were able to obtain the expected integral luminosity in the CLIC experiment to see a signal of a Z' with 95% C.L. or the discovery of a Z' with 5σ of statistical significance.

6 Perspective

In the future, we would like to delve further into phenomenological analyses and more advanced computational techniques in the context of future colliders. In particular, we intend to focus on the new physics reach of the Future Circular Collider (FCC) planned to be built at CERN. We will derive the FCC reach to new gauge symmetries such as $U(1)_{B-L}$ and dark matter particles. Moreover, we will assess FCC potential to probe lepton flavor violating interactions and compare our findings with searches for lepton flavor violation in muon decays. All these tasks will be conducted within the context of the FCC working group headed by CERN.

References

1 KLAUBER, R. D. *Student Friendly Quantum Field Theory:: Basic Principles and Quantum Electrodynamics.* Fairfield, Iowa: Sandtrove Press, 2013. ISBN 978-0-9845139-4-9. Cited on page 15.

2 MANDL, F.; SHAW, G. *QUANTUM FIELD THEORY.* [S.l.: s.n.], 1985. Cited 4 times on pages 15, 16, 27, and 30.

3 GIUNTI, C.; KIM, C. W. *Fundamentals of Neutrino Physics and Astrophysics.* [S.l.: s.n.], 2007. ISBN 978-0-19-850871-7. Cited 3 times on pages 15, 21, and 34.

4 QUIGG, C. *Gauge Theories of the Strong, Weak, and Electromagnetic Interactions: Second Edition.* USA: Princeton University Press, 2013. ISBN 978-0-691-13548-9, 978-1-4008-4822-5. Cited on page 16.

5 THOMSON, M. *Modern particle physics.* New York: Cambridge University Press, 2013. ISBN 978-1-107-03426-6. Cited 2 times on pages 18 and 21.

6 WU, C. S. et al. Experimental Test of Parity Conservation in β Decay. *Phys. Rev.*, v. 105, p. 1413–1414, 1957. Cited on page 21.

7 BAYES, R. et al. Experimental Constraints on Left-Right Symmetric Models from Muon Decay. *Phys. Rev. Lett.*, v. 106, p. 041804, 2011. Cited on page 21.

8 GLASHOW, S. L. Partial Symmetries of Weak Interactions. *Nucl. Phys.*, v. 22, p. 579–588, 1961. Cited on page 21.

9 WEINBERG, S. A Model of Leptons. *Phys. Rev. Lett.*, v. 19, p. 1264–1266, 1967. Cited on page 21.

10 SALAM, A. Elementary particle theory. *Prog. Of the Nobel Symposium, 1968, Stockholm, Sweden*, v. 367, 1968. Disponível em: <https://cir.nii.ac.jp/crid/1572543025734047488>. Cited on page 21.

11 PICH, A. The Standard Model of Electroweak Interactions. In: *2010 European School of High Energy Physics.* [S.l.: s.n.], 2012. p. 1–50. Cited on page 22.

12 WORKMAN, R. L. et al. Review of Particle Physics. *PTEP*, v. 2022, p. 083C01, 2022. Cited 3 times on pages 26, 34, and 37.

13 CHATRCHYAN, S. et al. Observation of a New Boson at a Mass of 125 GeV with the CMS Experiment at the LHC. *Phys. Lett. B*, v. 716, p. 30–61, 2012. Cited 2 times on pages 30 and 34.

14 AAD, G. et al. Observation of a new particle in the search for the Standard Model Higgs boson with the ATLAS detector at the LHC. *Phys. Lett. B*, v. 716, p. 1–29, 2012. Cited 2 times on pages 30 and 34.

15 MONTERO, J. C.; PIRES, C. A. de S.; PLEITEZ, V. Neutrino masses through a type II seesaw mechanism at TeV scale. *Phys. Lett.*, B502, p. 167–170, 2001. Cited on page 40.

16   TULLY, M. B.; JOSHI, G. C. Generating neutrino mass in the 331 model. *Phys. Rev.*, D64, p. 011301, 2001.   Cited 2 times on pages 40 and 61.

17   MONTERO, J. C.; PIRES, C. A. D. S.; PLEITEZ, V. Neutrino masses through the seesaw mechanism in 3-3-1 models. *Phys. Rev.*, D65, p. 095001, 2002.   Cited 2 times on pages 40 and 61.

18   CORTEZ, N. V.; TONASSE, M. D. Calculable lepton masses, seesaw relations and four neutrino mixings in a 3-3-1 model with extra U(1) symmetry. *Phys. Rev.*, D72, p. 073005, 2005.   Cited 2 times on pages 40 and 61.

19   COGOLLO, D.; DINIZ, H.; PIRES, C. A. de S. KeV right-handed neutrinos from type II seesaw mechanism in a 3-3-1 model. *Phys. Lett.*, B677, n. 5, p. 338–342, 2009. Cited 2 times on pages 40 and 61.

20   COGOLLO, D.; DINIZ, H.; PIRES, C. A. de S. Triple seesaw mechanism. *Phys. Lett.*, B687, p. 400–404, 2010.   Cited on page 40.

21   COGOLLO, D. et al. The Seesaw mechanism at TeV scale in the 3-3-1 model with right-handed neutrinos. *Eur. Phys. J.*, C58, p. 455–461, 2008.   Cited 2 times on pages 40 and 61.

22   OKADA, H.; OKADA, N.; ORIKASA, Y. Radiative seesaw mechanism in a minimal 3-3-1 model. *Phys. Rev.*, D93, n. 7, p. 073006, 2016.   Cited 2 times on pages 40 and 61.

23   VIEN, V. V.; LONG, H. N.; HERNáNDEZ, A. E. C. Lepton masses and mixings in a T' flavoured 3-3-1 model with type I and II seesaw mechanisms. *Mod. Phys. Lett.*, A34, n. 01, p. 1950005, 2019.   Cited on page 40.

24   HERNáNDEZ, A. E. C.; LONG, H. N.; VIEN, V. V. The first $\Delta(27)$ flavor 3-3-1 model with low scale seesaw mechanism. *Eur. Phys. J.*, C78, n. 10, p. 804, 2018.   Cited on page 40.

25   NGUYEN, T. P. et al. Decay of standard model-like Higgs boson $h \to \mu\tau$ in a 3-3-1 model with inverse seesaw neutrino masses. *Phys. Rev.*, D97, n. 7, p. 073003, 2018.   Cited on page 40.

26   PIRES, C. A. de S. et al. Implementing the inverse type-II seesaw mechanism into the 3-3-1 model. *Phys. Lett.*, B797, p. 134827, 2019.   Cited on page 40.

27   HERNáNDEZ, A. E. C.; PéREZ-JULVE, N. A.; VELáSQUEZ, Y. H. Fermion masses and mixings and some phenomenological aspects of a 3-3-1 model with linear seesaw mechanism. *Phys. Rev.*, D100, n. 9, p. 095025, 2019.   Cited on page 40.

28   HERNáNDEZ, A. E. C.; VELáSQUEZ, Y. H.; PéREZ-JULVE, N. A. A 3-3-1 model with low scale seesaw mechanisms. *Eur. Phys. J.*, C79, n. 10, p. 828, 2019.   Cited on page 40.

29   HERNáNDEZ, A. E. C. et al. *An extended 3-3-1 model with two scalar triplets and linear seesaw mechanism.* 2021.   Cited on page 40.

30   FREGOLENTE, D.; TONASSE, M. D. Selfinteracting dark matter from an SU(3)(L) x U(1)(N) electroweak model. *Phys. Lett.*, B555, p. 7–12, 2003.   Cited on page 40.

31 LONG, H. N.; LAN, N. Q. Selfinteracting dark matter and Higgs bosons in the SU(3)(C) x SU(3)(L) x U(1)(N) model with right-handed neutrinos. *Europhys. Lett.*, v. 64, p. 571, 2003. Cited on page 40.

32 PIRES, C. A. de S.; SILVA, P. S. Rodrigues da. Scalar Bilepton Dark Matter. *JCAP*, v. 0712, p. 012, 2007. Cited on page 40.

33 MIZUKOSHI, J. K. et al. WIMPs in a 3-3-1 model with heavy Sterile neutrinos. *Phys. Rev.*, D83, p. 065024, 2011. Cited 3 times on pages 40, 41, and 43.

34 RUIZ-ALVAREZ, J. D. et al. On the Connection of Gamma-Rays, Dark Matter and Higgs Searches at LHC. *Phys. Rev. D*, v. 86, p. 075011, 2012. Cited on page 40.

35 PROFUMO, S.; QUEIROZ, F. S. Constraining the Z' mass in 331 models using direct dark matter detection. *Eur. Phys. J.*, C74, n. 7, p. 2960, 2014. Cited on page 40.

36 DONG, P. V.; NGUYEN, T. P.; SOA, D. V. 3-3-1 model with inert scalar triplet. *Phys. Rev.*, D88, n. 9, p. 095014, 2013. Cited on page 40.

37 DONG, P. V.; HUNG, H. T.; THAM, T. D. 3-3-1-1 model for dark matter. *Phys. Rev.*, D87, n. 11, p. 115003, 2013. Cited on page 40.

38 COGOLLO, D. et al. Excluding the Light Dark Matter Window of a 331 Model Using LHC and Direct Dark Matter Detection Data. *JCAP*, v. 1411, n. 11, p. 002, 2014. Cited on page 40.

39 DONG, P. V. et al. Phenomenology of the 3-3-1-1 model. *Phys. Rev.*, D90, n. 7, p. 075021, 2014. Cited on page 40.

40 DONG, P. V.; NGAN, N. T. K.; SOA, D. V. Simple 3-3-1 model and implication for dark matter. *Phys. Rev.*, D90, n. 7, p. 075019, 2014. Cited on page 40.

41 KELSO, C. et al. Connection of $g - 2_\mu$, electroweak, dark matter, and collider constraints on 331 models. *Phys. Rev. D*, v. 90, n. 11, p. 113011, 2014. Cited on page 40.

42 MAMBRINI, Y.; PROFUMO, S.; QUEIROZ, F. S. Dark Matter and Global Symmetries. *Phys. Lett. B*, v. 760, p. 807–815, 2016. Cited on page 40.

43 DONG, P. V. et al. Investigation of Dark Matter in Minimal 3-3-1 Models. *Phys. Rev. D*, v. 91, n. 11, p. 115019, 2015. Cited on page 40.

44 PIRES, C. A. de S. et al. Higgs mass and right-handed sneutrino WIMP in a supersymmetric 3-3-1 model. *Phys. Rev. D*, v. 94, n. 5, p. 055014, 2016. Cited on page 40.

45 ALVES, A. et al. Matter-parity as a residual gauge symmetry: Probing a theory of cosmological dark matter. *Phys. Lett. B*, v. 772, p. 825–831, 2017. Cited on page 40.

46 SILVA, P. S. Rodrigues da. A Brief Review on WIMPs in 331 Electroweak Gauge Models. *Phys. Int.*, v. 7, n. 1, p. 15–27, 2016. Cited on page 40.

47 CARVAJAL, C. D. R.; SáNCHEZ-VEGA, B. L.; ZAPATA, O. Linking axionlike dark matter to neutrino masses. *Phys. Rev.*, D96, n. 11, p. 115035, 2017. Cited on page 40.

48 DONG, P. V. et al. The Dark Side of Flipped Trinification. *JHEP*, v. 04, p. 143, 2018. Cited on page 40.

49 ARCADI, G. et al. Lepton Flavor Violation Induced by Dark Matter. *Phys. Rev. D*, v. 97, n. 7, p. 075022, 2018. Cited on page 40.

50 MONTERO, J. C.; ROMERO, A.; SáNCHEZ-VEGA, B. L. Axion dark matter in a $3 - 3 - 1$ model. *Phys. Rev.*, D97, n. 6, p. 063015, 2018. Cited on page 40.

51 HUONG, D. T. et al. Dark matter and flavor changing in the flipped 3-3-1 model. *JHEP*, v. 08, p. 051, 2019. Cited on page 40.

52 ALVAREZ-SALAZAR, C. E.; PERES, O. L. G. Constraining the $3 - 3 - 1$ model with heavy neutral leptons using $(g - 2)_\mu$ and dark matter observables. *Phys. Rev. D*, v. 103, n. 3, p. 035029, 2021. Cited on page 40.

53 LOI, D. V.; NAM, C. H.; DONG, P. V. Dark matter in the fully flipped 3-3-1-1 model. *Eur. Phys. J. C*, v. 81, n. 7, p. 591, 2021. Cited on page 40.

54 DUTRA, M. et al. A model for mixed warm and hot right-handed neutrino dark matter. *JHEP*, v. 10, p. 005, 2021. Cited on page 40.

55 OLIVEIRA, V.; PIRES, C. A. d. S. Pandax-4T limits on Z' mass in 3-3-1LHN model. 12 2021. Cited on page 40.

56 COGOLLO, D. et al. Novel sources of Flavor Changed Neutral Currents in the 331_{RHN} model. *Eur. Phys. J. C*, v. 72, p. 2029, 2012. Cited on page 40.

57 COGOLLO, D.; QUEIROZ, F. S.; VASCONCELOS, P. Flavor Changing Neutral Current Processes in a Reduced Minimal Scalar Sector. *Mod. Phys. Lett. A*, v. 29, n. 32, p. 1450173, 2014. Cited on page 40.

58 BURAS, A. J.; FAZIO, F. D.; GIRRBACH-NOE, J. Z-Z' mixing and Z-mediated FCNCs in $SU(3)_C \times SU(3)_L \times U(1)_X$ models. *JHEP*, v. 08, p. 039, 2014. Cited on page 40.

59 BURAS, A. J.; FAZIO, F. D. ε'/ε in 331 Models. *JHEP*, v. 03, p. 010, 2016. Cited on page 40.

60 QUEIROZ, F. S.; SIQUEIRA, C.; VALLE, J. W. F. Constraining Flavor Changing Interactions from LHC Run-2 Dilepton Bounds with Vector Mediators. *Phys. Lett. B*, v. 763, p. 269–274, 2016. Cited on page 40.

61 MELO, T. B. de et al. Rare kaon decay to missing energy: Implications of the NA62 result for a Z model. *Phys. Rev. D*, v. 103, n. 11, p. 115001, 2021. Cited on page 40.

62 BURAS, A. J.; FAZIO, F. D. 331 Models Facing the Tensions in $\Delta F = 2$ Processes with the Impact on ε'/ε, $B_s \to \mu^+\mu^-$ and $B \to K^*\mu^+\mu^-$. *JHEP*, v. 08, p. 115, 2016. Cited on page 40.

63 BURAS, A. J. et al. The charm of 331. *JHEP*, v. 10, p. 021, 2021. Cited on page 40.

64 CABARCAS, J. M.; DUARTE, J.; RODRIGUEZ, J. A. Lepton Flavor Violation processes in 331 Models. *PoS*, HQL2012, p. 072, 2012. Cited on page 40.

65 HUE, L. T. et al. Exact one-loop results for $l_i \to l_j\gamma$ in 3-3-1 models. *Eur. Phys. J.*, C78, n. 2, p. 128, 2018. Cited on page 40.

66 MONTERO, J. C.; SANCHEZ-VEGA, B. L. Natural PQ symmetry in the 3-3-1 model with a minimal scalar sector. *Phys. Rev.*, D84, p. 055019, 2011. Cited on page 40.

67 SANTOS, A. C. O.; VASCONCELOS, P. Lower Mass Bound on the W' mass via Neutrinoless Double Beta Decay in a 3-3-1 Model. *Adv. High Energy Phys.*, v. 2018, p. 9132381, 2018. Cited on page 40.

68 BARRETO, E. R. et al. Hierarchical fermions and detectable Z from effective two-Higgs-triplet 3-3-1 model. *Phys. Rev.*, D97, n. 5, p. 055047, 2018. Cited on page 40.

69 CONTO, G. D.; MACHADO, A. C. B.; MELO, J. P. B. C. de. The Higgs boson in the minimal 3-3-1 model. *Phys. Lett.*, B784, p. 255–260, 2018. Cited on page 40.

70 CHEN, N.; LIU, Y.; TENG, Z. Axion model with the SU(6) unification. *Phys. Rev. D*, v. 104, n. 11, p. 115011, 2021. Cited on page 40.

71 CHEN, N.; MAO, Y.-n.; TENG, Z. Bottom quark and tau lepton masses in a toy $SU(6)$. 12 2021. Cited on page 40.

72 ARCADI, G. et al. The waning of the WIMP? A review of models, searches, and constraints. *Eur. Phys. J. C*, v. 78, n. 3, p. 203, 2018. Cited on page 40.

73 CATANO, M. E.; MARTINEZ, R.; OCHOA, F. Neutrino masses in a 331 model with right-handed neutrinos without doubly charged Higgs bosons via inverse and double seesaw mechanisms. *Phys. Rev.*, D86, p. 073015, 2012. Cited on page 41.

74 LONG, H. N. SU(3)-L x U(1)-N model for right-handed neutrino neutral currents. *Physical Review D*, D54, n. 7, p. 4691–4693, 1996. Cited on page 41.

75 LONG, H. N. The 331 model with right handed neutrinos. *Phys. Rev.*, D53, p. 437–445, 1996. Cited on page 41.

76 ALWALL, J. et al. The automated computation of tree-level and next-to-leading order differential cross sections, and their matching to parton shower simulations. *Journal of High Energy Physics*, Springer Science and Business Media LLC, v. 2014, n. 7, p. 1–157, 2014. Disponível em: <http://dx.doi.org/10.1007/JHEP07(2014)079>. Cited 2 times on pages 47 and 62.

77 FREDERIX, R. et al. The automation of next-to-leading order electroweak calculations. *Journal of High Energy Physics*, Springer, v. 2018, n. 7, p. 1–121, 2018. Disponível em: <http://dx.doi.org/10.1007/JHEP07(2018)185>. Cited on page 47.

78 BELYAEV, A.; CHRISTENSEN, N. D.; PUKHOV, A. Calchep 3.4 for collider physics within and beyond the standard model. *Computer Physics Communications*, Elsevier, v. 184, n. 7, p. 1729–1769, 2013. Cited on page 47.

79 PUKHOV, A.; BELYAEV, A.; CHRISTENSEN, N. *CalcHep*. Accessed: 2021–09–20. <https://theory.sinp.msu.ru/~pukhov/calchep.html>. Cited on page 47.

80 COLLABORATION, A. et al. Search for high-mass dilepton resonances using 139 fb- 1 of pp collision data collected at s= 13 tev with the atlas detector. *Physics Letters B*, v. 796, p. 68–87, 2019. ISSN 0370-2693. Disponível em: <https://www.sciencedirect.com/science/article/pii/S0370269319304721>. Cited 2 times on pages 47 and 52.

81 CARRAZZA, S.; FORTE, S.; ROJO, J. Parton Distributions and Event Generators. In: *43rd International Symposium on Multiparticle Dynamics.* [S.l.: s.n.], 2013. p. 89–96. Cited on page 47.

82 ALLOUL, A. et al. Feynrules 2.0—a complete toolbox for tree-level phenomenology. *Computer Physics Communications*, Elsevier BV, v. 185, n. 8, p. 2250–2300, 2014. Disponível em: <http://dx.doi.org/10.1016/j.cpc.2014.04.012>. Cited on page 47.

83 ALLOUL, A. et al. *FeynRules*. Accessed: 2021–09–20. <https://feynrules.irmp.ucl.ac. be/>. Cited 2 times on pages 47 and 62.

84 DIAS, A. G.; PIRES, C. A. de S.; SILVA, P. S. Rodrigues da. Naturally light right-handed neutrinos in a 3-3-1 model. *Phys. Lett. B*, v. 628, p. 85–92, 2005. Cited on page 52.

85 CEPEDA, M. et al. Report from Working Group 2: Higgs Physics at the HL-LHC and HE-LHC. *CERN Yellow Rep. Monogr.*, v. 7, p. 221–584, 2019. Cited on page 53.

86 ABADA, A. et al. FCC Physics Opportunities: Future Circular Collider Conceptual Design Report Volume 1. *Eur. Phys. J. C*, v. 79, n. 6, p. 474, 2019. Cited on page 53.

87 BRUNNER, O. et al. The CLIC project. 3 2022. Cited 2 times on pages 58 and 60.

88 ROLANDI, G. LEP results. In: *Summer School in High-energy Physics and Cosmology (Includes Workshop on Strings, Gravity, and Related Topics 29-30 Jul 1993).* [S.l.: s.n.], 1995. p. 1–13. Cited 2 times on pages 58 and 60.

89 GURTU, A. Recent results from LEP. *Pramana*, v. 54, p. 455–470, 2000. Cited 2 times on pages 58 and 60.

90 HEECK, J.; RODEJOHANN, W. Gauged $L_\mu - L_\tau$ Symmetry at the Electroweak Scale. *Phys. Rev. D*, v. 84, p. 075007, 2011. Cited on page 59.

91 AGUILA, F. del et al. Collider limits on leptophilic interactions. *JHEP*, v. 03, p. 059, 2015. Cited on page 59.

92 BELL, N. F. et al. Leptophilic dark matter with Z interactions. *Phys. Rev. D*, v. 90, n. 3, p. 035027, 2014. Cited on page 59.

93 KARA, S. O.; AKKOYUN, S.; BAYRAM, T. Probing for leptophilic gauge boson Z_l ILC with $\sqrt{s} = 1$ TeV by using ANN. *Int. J. Mod. Phys. A*, v. 29, n. 30, p. 1450171, 2014. Cited on page 59.

94 PATRA, S. et al. Gauged $U(1)_{L_\mu - L_\tau}$ model in light of muon $g - 2$ anomaly, neutrino mass and dark matter phenomenology. *Nucl. Phys. B*, v. 917, p. 317–336, 2017. Cited on page 59.

95 HEECK, J. Lepton flavor violation with light vector bosons. *Phys. Lett. B*, v. 758, p. 101–105, 2016. Cited on page 59.

96 ALTMANNSHOFER, W. et al. Lepton flavor violating Z' explanation of the muon anomalous magnetic moment. *Phys. Lett. B*, v. 762, p. 389–398, 2016. Cited on page 59.

97 ALTMANNSHOFER, W. et al. Explaining dark matter and B decay anomalies with an $L_\mu - L_\tau$ model. *JHEP*, v. 12, p. 106, 2016. Cited on page 59.

98 SADHUKHAN, S.; SINGH, M. P. Neutrino floor in leptophilic $U(1)$ models: Modification in $U(1)_{L_\mu - L_\tau}$. *Phys. Rev. D*, v. 103, n. 1, p. 015015, 2021. Cited on page 59.

99 ANCHORDOQUI, L. A. et al. Leptophilic U(1) massive vector bosons from large extra dimensions. *Phys. Lett. B*, v. 820, p. 136585, 2021. Cited on page 59.

100 ASAI, K.; MOROI, T.; NIKI, A. Leptophilic Gauge Bosons at ILC Beam Dump Experiment. *Phys. Lett. B*, v. 818, p. 136374, 2021. Cited on page 59.

101 MOROI, T.; NIKI, A. Leptophilic gauge bosons at lepton beam dump experiments. *JHEP*, v. 05, p. 016, 2023. Cited on page 59.

102 KO, P.; OMURA, Y. Supersymmetric U(1)B x U(1)L model with leptophilic and leptophobic cold dark matters. *Phys. Lett. B*, v. 701, p. 363–366, 2011. Cited on page 59.

103 KARA, S. O. et al. A Search for leptophilic $Z_{(}l)$ boson at future linear colliders. *JHEP*, v. 08, p. 072, 2011. Cited on page 59.

104 ALLANACH, B. et al. Z models for the LHCb and $g - 2$ muon anomalies. *Phys. Rev. D*, v. 93, n. 5, p. 055045, 2016. [Erratum: Phys.Rev.D 95, 119902 (2017)]. Cited on page 59.

105 BURAS, A. J. et al. Global analysis of leptophilic Z' bosons. *JHEP*, v. 06, p. 068, 2021. Cited 2 times on pages 59 and 61.

106 LI, Y.-Y. et al. The light leptophilic gauge boson Zx and the leptonic decays of charged pseudoscalar mesons. *Nucl. Phys. B*, v. 982, p. 115899, 2022. Cited on page 59.

107 CHUN, E. J.; MONDAL, T. Leptophilic bosons and muon g-2 at lepton colliders. *JHEP*, v. 07, p. 044, 2021. Cited on page 59.

108 LI, J. et al. A Comparative Study of Z′ mediated Charged Lepton Flavor Violation at future lepton colliders. 2 2023. Cited on page 59.

109 SOA, D. V. et al. Single Z-prime production at CLIC based on e- gamma collisions. *J. Exp. Theor. Phys.*, v. 98, p. 661–666, 2004. Cited on page 59.

110 BLAISING, J.-J.; WELLS, J. D. Physics performances for Z' searches at 3 TeV and 1.5 TeV CLIC. 8 2012. Cited on page 59.

111 SPOR, S.; GURKANLI, E.; KÖKSAL, M. Search for the anomalous ZZγ and Z$\gamma\gamma$ couplings via $\nu\nu\gamma$ production at the CLIC. *Nucl. Phys. B*, v. 979, p. 115785, 2022. Cited on page 59.

112 İNAN, S. C.; KISSELEV, A. V. Probing anomalous $\gamma\gamma\gamma Z$ couplings through γZ production in $\gamma\gamma$ collisions at the CLIC. *JHEP*, v. 10, p. 121, 2021. Cited on page 59.

113 GURKANLI, E. Sensitivities on the anomalous quartic $\gamma\gamma\gamma\gamma$ and $\gamma\gamma\gamma Z$ couplings at the CLIC. 7 2023. Cited on page 59.

114 Physics and Detectors at CLIC: CLIC Conceptual Design Report. 2 2012. Cited on page 60.

115 ASLANIDES, E. et al. *Charting the European Course to the High-Energy Frontier.* [S.l.], 2019. Contribution to the update of the European Strategy for Particle Physics. Disponível em: <https://cds.cern.ch/record/2706890>. Cited on page 60.

116 ROBSON, A.; ROLOFF, P. Updated CLIC luminosity staging baseline and Higgs coupling prospects. 12 2018. Cited on page 60.

117 FRANCESCHINI, R. Beyond the Standard Model physics at CLIC. *Int. J. Mod. Phys. A*, v. 35, n. 15n16, p. 2041015, 2020. Cited on page 60.

118 SICKING, E.; STRÖM, R. From precision physics to the energy frontier with the Compact Linear Collider. *Nature Phys.*, v. 16, n. 4, p. 386–392, 2020. Cited on page 60.

119 ZARNECKI, A. F. On the physics potential of ILC and CLIC. *PoS*, CORFU2019, p. 037, 2020. Cited on page 60.

120 ACCOMANDO, E. et al. Physics at the CLIC multi-TeV linear collider. In: *11th International Conference on Hadron Spectroscopy.* [S.l.: s.n.], 2004. (CERN Yellow Reports: Monographs). Cited on page 60.

121 BLAS, J. de et al. The CLIC Potential for New Physics. v. 3/2018, 12 2018. Cited on page 60.

122 ALVES, A. et al. Constraining 3-3-1 models at the LHC and future hadron colliders. *Phys. Rev. D*, v. 106, n. 5, p. 055027, 2022. Cited on page 61.

123 HE, X.-G. et al. Simplest Z-prime model. *Phys. Rev. D*, v. 44, p. 2118–2132, 1991. Cited on page 61.

124 SJOSTRAND, T.; MRENNA, S.; SKANDS, P. Z. A Brief Introduction to PYTHIA 8.1. *Comput. Phys. Commun.*, v. 178, p. 852–867, 2008. Cited on page 62.

125 FAVEREAU, J. de et al. DELPHES 3, A modular framework for fast simulation of a generic collider experiment. *JHEP*, v. 02, p. 057, 2014. Cited on page 62.